

Cost-Effective Condition Monitoring for Wind Turbines

Wenxian Yang, Peter J. Tavner, *Senior Member, IEEE*, Christopher J. Crabtree, and Michael Wilkinson

Abstract—Cost-effective wind turbine (WT) condition monitoring assumes more importance as turbine sizes increase and they are placed in more remote locations, for example, offshore. Conventional condition monitoring techniques, such as vibration, lubrication oil, and generator current signal analysis, require the deployment of a variety of sensors and computationally intensive analysis techniques. This paper describes a WT condition monitoring technique that uses the generator output power and rotational speed to derive a fault detection signal. The detection algorithm uses a continuous-wavelet-transform-based adaptive filter to track the energy in the prescribed time-varying fault-related frequency bands in the power signal. The central frequency of the filter is controlled by the generator speed, and the filter bandwidth is adapted to the speed fluctuation. Using this technique, fault features can be extracted, with low calculation times, from direct- or indirect-drive fixed- or variable-speed WTs. The proposed technique has been validated experimentally on a WT drive train test rig. A synchronous or induction generator was successively installed on the test rig, and both mechanical and electrical fault-like perturbations were successfully detected when applied to the test rig.

Index Terms—Adaptive signal processing, condition monitoring, fault diagnosis, induction generators, signal processing, synchronous generators, time-frequency analysis, wavelet transforms, wind power generation.

NOMENCLATURE

A	Estimated energy of the frequency component of interest.
a_{\min}, a_{\max}	Minimum and maximum wavelet scales considered by the adaptive bandpass filter.
a	Wavelet scale.
b	Wavelet time-shift parameter.
ε	Voltage or current transducer error.
e	Specific unbalance.
f_{rm}	Rotational frequency of the generator rotor.
f_{se}	Electrical supply frequency.

G	Balance quality grade.	41
I_i	Line currents.	42
m	Unbalanced mass.	43
M_{eq}	Equivalent mass of the test rig rotor.	44
ω	Angular frequency of interest.	45
ω_c	Mean frequency of the prescribed frequency component during the time interval T .	46–47
ω_{fg}	Fluctuation of the generator rotational frequency.	48–49
ω_f	Fluctuation of the frequency of interest.	50–51
$\omega_{upper}, \omega_{lower}$	Upper and lower cutoff frequencies of the adaptive filter.	52–53
ω_0	Central angular frequency of the mother wavelet.	54–55
ω_{rm}	Angular rotational frequency of the generator rotor.	56–57
P	Three-phase total power output from the generator.	58–59
r	Effective radius of the equivalent unbalanced mass.	60–61
R_{AB}, R_{BC}, R_{CA}	Combined line-to-line resistances.	62
R_{AS}, R_{BS}, R_{CS}	Brush gear and slip ring resistances.	63
R_{AV}, R_{BV}, R_{CV}	Load bank resistances.	64
R_A, R_B, R_C	Generator rotor winding resistances.	65
δR	Electrical resistance imbalance.	66
s	Induction machine slip.	67
ψ	Mother wavelet function.	68
T	Sliding window averaging time interval.	69
t_0	Starting time moment of the sliding window.	70–71
U_e	Electrical asymmetry on the generator rotor.	72–73
U_m	Mechanical unbalance on the generator rotor.	74–75
V_i	Phase voltages.	76
x	Real-time signal.	77
η	Constant between ω_{fg} and ω_f .	78

Manuscript received December 5, 2008; revised September 3, 2009. This work was supported by the U.K. Engineering and Physical Sciences Research Council Supergen Wind Program EP/D034566/1.

W. Yang is with the New and Renewable Energy Centre, NE24 3AG Blyth, U.K.

P. J. Tavner is with the School of Engineering and Computing Sciences, Durham University, DH1 3LE Durham, U.K., and also with the New and Renewable Energy Centre, NE24 3AG Blyth, U.K. (e-mail: Peter.Tavner@durham.ac.uk).

C. J. Crabtree is with Durham University, DH1 3LE Durham, U.K.

M. Wilkinson is with Garrad Hassan, BS2 0QD Bristol, U.K.

Color versions of one or more of the figures in this paper are available online at <http://ieeexplore.ieee.org>.

Digital Object Identifier 10.1109/TIE.2009.2032202

I. INTRODUCTION 79

OVER THE last 40 years, there has been an increased application of wind turbines (WTs) around the world, 81 with growth in rating from 30 kW to > 5 MW and, more 82 recently, their application offshore [1]. To reduce the cost of 83 energy from WTs, there is a pressing need to improve the WT 84 availability and reduce the operational and maintenance (O&M) 85

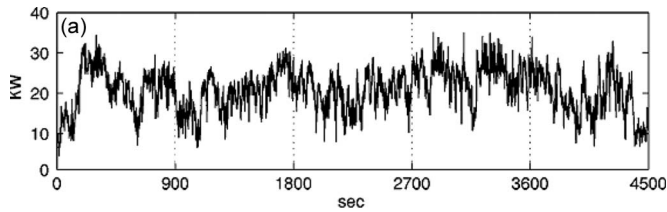


Fig. 1. Variation in power output from a 33-kW fixed-speed WT over five successive periods of 900 s, each showing the large variation in the signal due to wind turbulence (taken from [7]).

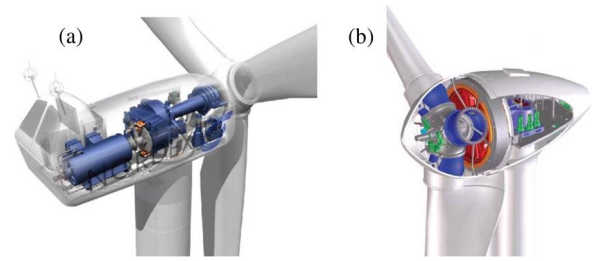


Fig. 2. Structures of real large WTs. (a) Geared. (b) Direct drive.

86 costs. Aside from developing more advanced machine designs
87 [2] to improve the availability, an effective way to achieve
88 this improvement would be to apply reliable and cost-effective
89 condition monitoring [3], which is why this subject is attracting
90 industrial and academic attention.

91 The wind industry currently uses condition monitoring sys-
92 tems (CMSs), such as vibration, temperature, lubrication oil,
93 and generator current analysis, developed from other rotating
94 machine power generation industries [4]–[6], where they have
95 achieved success. However, despite their application in the
96 wind industry [7], they have not yet proven their effectiveness
97 due to the peculiarities of a WT, which has a slow speed and
98 rapidly varying torque. Commercial WT CMSs mostly employ
99 vibration-based techniques, which are sophisticated, and the
100 sensors and cabling are costly. The technique is also not ideally
101 suited to all WT types and faults. Lubrication oil analysis is
102 becoming more popular for detecting gearbox tooth and bearing
103 wear but cannot detect failures outside the gearbox. More
104 advanced techniques, such as optical strain measurement, have
105 been developed for monitoring WT blade integrity. However,
106 these are expensive, and recent reliability surveys [8] have
107 shown that WT electrical systems have a higher failure rate than
108 the mechanical systems. For these reasons, an electrically based
109 WT CMS would be beneficial and could be more comprehen-
110 sive, simpler, and cheaper than other techniques. This paper will
111 propose such a technique.

112 Instantaneous electric power measurement has been demon-
113 strated on induction machines for detecting motor faults [9].
114 Three-phase total power monitoring has also been applied to
115 WTs as a condition monitoring and fault diagnosis signal [10]
116 but has not achieved commercial application. This research will
117 be based entirely on the use of this signal and the generator
118 speed for condition monitoring. Power output measurement
119 was considered for condition monitoring in [7] and [10], but
120 Fig. 1, taken from [7], shows how the WT power output signal
121 experiences continuous and rapid variations during operation.

122 The work reported in this paper is an enhancement of the
123 research described in [11], now including the following:

- 124 1) a more comprehensive description of the background
125 technology and the state of the art of the proposed
126 technique;
- 127 2) an improved mathematical presentation;
- 128 3) additional figures to enhance the description of the
129 technique;
- 130 4) more substantial experimental results;
- 131 5) an amended conclusion.

The novelties of the proposed technique are summarized as 132
follows: 133

- 1) a technique for WT condition monitoring based on mea- 134
suring the generator total power signal rather than more 135
conventional measurements validated by experiments on 136
a test rig with a simple fault setup; 137
- 2) a new adaptive continuous-wavelet-transform (CWT)- 138
based energy tracking method, reducing the calculation 139
time for feature extraction when applied to lengthy sig- 140
nals, making possible less time-intensive WT condition 141
monitoring; 142
- 3) the successful detection of two types of fault using this 143
method has been demonstrated on two WT arrangements, 144
including both electrical and mechanical faults; 145
- 4) the proposed method is more efficient for the detection 146
of faults in variable-speed WTs than other more conven- 147
tional techniques; 148
- 5) the technique used in this paper can be applied to any WT 149
generator for tracking any characteristic, fault-related fre- 150
quency component, so it is general and could be applied 151
to detect a variety of faults depending on the choice of 152
frequency selected. 153

Wavelet transforms have been successfully used in condition 154
monitoring and diagnosis of rotating electrical machine faults 155
[1], [12]–[14]. However, most used the discrete wavelet trans- 156
form (DWT) rather than the CWT, although the latter is superior 157
to the former in multiresolution signal analysis. However, the 158
CWT involves more intensive convolution calculations than the 159
DWT, making it more difficult to process lengthy online data, 160
such as WT monitoring signals. Moreover, it is inconvenient to 161
apply the traditional time–frequency–amplitude CWT image to 162
machine condition monitoring, as was done in [15]. Wavelets 163
have been proposed for WT condition monitoring [16], [17] but 164
have not yet received commercial application. 165

II. APPLYING GENERATOR POWER MONITORING TO WTs 166

A WT converts the kinetic energy of the wind into electrical 167
energy, utilizing mechanical and electrical conversion, control, 168
and transmission systems. The architectures of two commonly 169
used large WTs are shown in Fig. 2. 170

The application of vibration, temperature, and lubrication oil 171
techniques to monitoring WTs should improve their availability 172
but, to date, is not being widely used for the following reasons: 173

- 1) lack of practical industry experience with condition mon- 174
itoring in the wind environment; 175
- 2) difficulties collecting and interpreting the data, including 176
the risk of false or missed alarms; 177

178 3) the fact that present techniques may not be suited to all
179 types of WTs such as shown in Fig. 2;

180 4) the fact that developing reliable WT condition monitoring
181 techniques requires complex and lengthy collaboration
182 between WT operators and manufacturers in the field.

183 WT power flows are disturbed by both mechanical and
184 electrical faults [16], [17]. To measure the WT shaft torque is
185 costly and usually impractical for a real WT. In contrast, shaft
186 speed and electrical power output are routinely monitored for
187 WTs, but, to date, commercial CMSs do not use these signals.
188 In comparison with conventional stator current analysis,
189 widely adopted for condition monitoring motors [4], [6], power
190 monitoring could have the following disadvantages.

191 1) The error in the total power signal depends not only on
192 the voltage and current transducer error ε but also on the
193 measurement method. In the three-wattmeter method, the
194 error will be 6ε , but, in the two-wattmeter method,
195 the error is limited to 4ε , whereas the current signal error
196 would be only ε . Therefore, the signal-to-noise ratio for
197 basic analysis should be better for current than power
198 analysis.

199 On the other hand, monitoring based on power analysis could
200 have the following advantages.

201 1) The power signal is already available from the generator
202 terminal voltage and current signals for the control of the
203 WT and can conveniently be accessed.

204 2) Fewer cheaper transducers than accelerometers and oil
205 debris probes are required for power monitoring.

206 3) Mechanical and electrical faults both disturb the genera-
207 tor power output, so power monitoring could detect both
208 types of faults.

209 4) Single line current analysis contains the mains frequency
210 carrier, whereas this is absent in the power signal. There-
211 fore, the signal-to-noise ratio for faulty feature analysis
212 should be better for power than current analysis, balanc-
213 ing the aforementioned transducer error effect.

214 5) In the power signal, the fault-related frequency side-
215 bands, around the mains frequency, are folded down
216 around dc, limiting the bandwidth needed to monitor the
217 signal.

218 An example of the current, voltage, and power signals mea-
219 sured under faulty conditions on an induction generator, fitted to
220 the test rig described in the following, is shown in Fig. 3, where
221 the signals were collected when a periodic rotor electrical
222 asymmetry was applied in the presence of serious noise due
223 to power system imbalance.

224 The fault in Fig. 3 was applied at the time intervals of 20–40 s
225 and 60–80 s and was absent in the other time intervals. It
226 can be seen that the amplitudes of both the current–time and
227 voltage–time waveforms gave no indication of abnormal con-
228 ditions, whereas the total three-phase power signal P changes
229 significantly during the abnormality due to the presence of $2f_{se}$
230 and $2sf_{se}$ components. The total power $P(t)$ was calculated
231 using

$$P(t) = \sum_{i=1}^3 I_i(t) \cdot V_i(t). \quad (1)$$

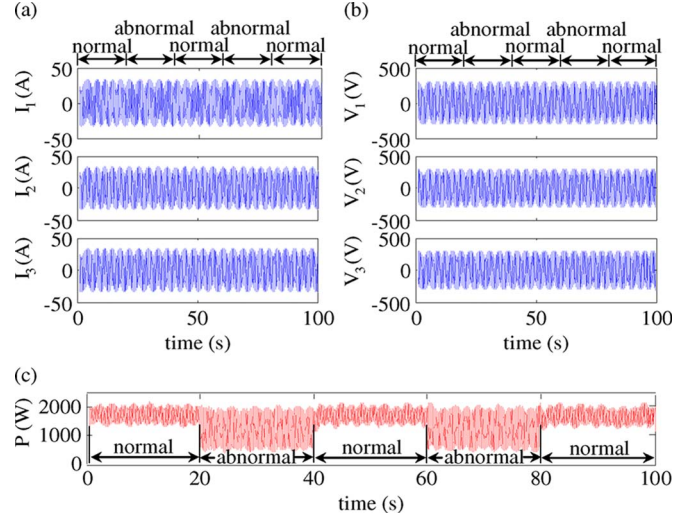


Fig. 3. Comparison of current, voltage, and total power signal in the presence of a rotor asymmetry fault. (a) Line currents. (b) Phase voltages. (c) Total power.

III. DESIGN OF WAVELET-BASED ADAPTIVE FILTER 232

In this paper, a CWT-based adaptive filter has been designed 233 to track the energy in the power signal in the prescribed fault- 234 related frequency bands rather than at all frequencies of the 235 monitoring signal. In this way, the wavelet calculation can 236 significantly be reduced, and the results can be displayed graph- 237 ically rather than as a screen dump image, making the technique 238 attractive for online application. Details of the technique are 239 described as follows. 240

The CWT of a real-time signal $x(t)$ can be defined as 241

$$\text{CWT}(b, a) = \frac{1}{\sqrt{|a|}} \int_{-\infty}^{\infty} x(t) \psi^* \left(\frac{t-b}{a} \right) dt \quad (2)$$

where the asterisk “*” indicates the complex conjugate. 242

Traditionally, the wavelet function $\psi(t)$ is dilated or com- 243 pressed by changing the scale parameter a so that all signal 244 components ranging from frequency 0 to half the sampling 245 frequency can be projected onto an appropriate time-scale map, 246 as shown in Fig. 4. The bottom figure shows the time waveform 247 of a sample signal of increasing frequency being inspected; the 248 top figure shows the wavelet coefficients of this signal obtained 249 at different wavelet scales and times. 250

Many of the calculations shown in Fig. 4 are unnecessary for 251 WT condition monitoring because the fault-related frequencies 252 are few in number and the energy extracted at nonfault-related 253 frequencies is not helpful to assess the machine condition. 254

Therefore, an adaptive CWT-based filter has been designed, 255 which only extracts energy at known fault frequencies, while 256 frequencies unrelated to the fault are left unprocessed. The 257 calculation time for the new technique will be much shorter 258 than that for a conventional CWT applied to a broad band- 259 width signal. Therefore, the proposed CWT-based energy 260 tracking technique should prove more efficient for online 261 processing of WT monitoring signals than conventional CWT 262 processing. 263

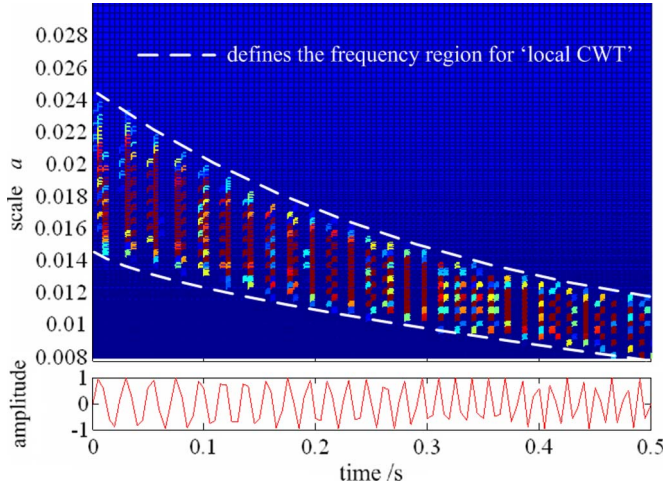


Fig. 4. Illustrative example of the conventional CWT.

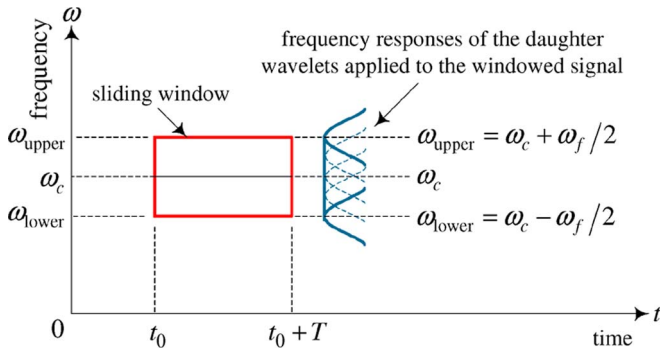


Fig. 5. Two-dimensional sliding window.

264 A time–frequency sliding window has been designed for this
265 task, as shown in Fig. 5. Its central frequency ω_c is the mean
266 frequency during the time interval T of the prescribed fault-
267 related frequency band. The upper and lower cutoff frequencies
268 ω_{upper} and ω_{lower} are adapted to the fluctuation of the generator
269 rotational speed ω_{fg} in that interval, i.e.,

$$\begin{cases} \omega_{\text{upper}} = \omega_c + \omega_f/2 \\ \omega_{\text{lower}} = \omega_c - \omega_f/2 \\ \omega_f = \eta\omega_{\text{fg}}. \end{cases} \quad (3)$$

270 From Fig. 4, it is noticed that ω_f could also be a time-
271 varying parameter, intrinsically dependent on the turbulence of
272 the wind. Experience has shown that onshore wind turbulence
273 varies between 12% and 20%, whereas offshore turbulence
274 approximates to $\sim 6\%$.

275 The relationship between any prescribed frequency ω and its
276 corresponding wavelet scale a is

$$a = \frac{\omega_0}{\omega}. \quad (4)$$

277 With the aid of (3) and (4), the range of the wavelet scales
278 for conducting bandpass filtering can be determined by

$$a \in [a_{\text{min}} \quad a_{\text{max}}] \quad (5)$$

$$\begin{cases} a_{\text{min}} = \frac{\omega_0}{\omega_{\text{upper}}} \\ a_{\text{max}} = \frac{\omega_0}{\omega_{\text{lower}}}. \end{cases} \quad (6)$$

TABLE I
COMPUTATIONAL EFFICIENCY COMPARISON BETWEEN CWT, DWT,
AND PROPOSED APPROACH

Method	Time cost	Operation manner	Accuracy
CWT	18.91s	All frequencies between zero and half sampling frequency are calculated.	Good
DWT	0.31s	Interested frequency band is determined in a rigid dyadic step way.	Not good
Energy tracking	0.16s	Interested frequency band is determined intelligently.	As good as CWT

Subsequently, by performing the CWT locally in the scale 279
range defined by (5), a matrix of wavelet coefficients is obtained 280

$$\text{CWT}_{\text{local}}(b, a) = \frac{1}{\sqrt{|a|}} \int_{-\infty}^{\infty} x(t) \psi^* \left(\frac{t-b}{a} \right) dt. \quad (7)$$

The energy A of the frequency component of interest in the 281
time interval T is estimated by 282

$$A(t_0 + T/2) = \max(|\text{CWT}_{\text{local}}(b, a)|) \quad \begin{cases} a \in [a_{\text{min}} \quad a_{\text{max}}] \\ b \in [t_0 \quad t_0 + T]. \end{cases} \quad (8)$$

The sliding window is moved forward along the signal; the 283
maximum and minimum wavelet scales in (5) being redefined 284
within each time interval according to the generator rotational 285
speed ω_{fg} . Then, using the aforementioned technique, the en- 286
ergy A in the fault-related frequency band is calculated in each 287
time interval using (7) and (8). These calculations are repeated 288
until the whole signal has been processed. Finally, a curve 289
of the energy variation in the fault-related frequency band is 290
obtained, and changes in the running condition of the WT can 291
be assessed. 292

This task could have been accomplished using a series of 293
conventional bandpass filters set up to cover the expected speed 294
range of the turbine. However, such an analysis would not have 295
the advantages of the CWT in processing nonstationary signals 296
shown in Fig. 1 and [18]. 297

To verify the computational efficiency of the proposed tech- 298
nique compared to the traditional CWT and DWT, a calculation 299
was performed to extract the 50-Hz energy component from 300
1 s of line current signal, sampled at a frequency of 2 kHz. 301
The time taken by each approach is listed in Table I. The 302
calculations were done in a computer with 1.4 GHz of Intel 303
Pentium processor and 512 MB of RAM. 304

From Table I, it can be concluded that the proposed energy 305
tracking technique is the most computationally efficient of the 306
three approaches. 307

IV. WT CONDITION MONITORING BY POWER SIGNAL ANALYSIS 308 309

In view of the proposed advantages of generator power 310
signal analysis for detecting both mechanical and electrical 311
faults in a variety of designs of WT drive train, it has been 312
applied in this paper, in combination with the energy tracking 313
method described previously, to develop a new WT condition 314
monitoring technique. 315

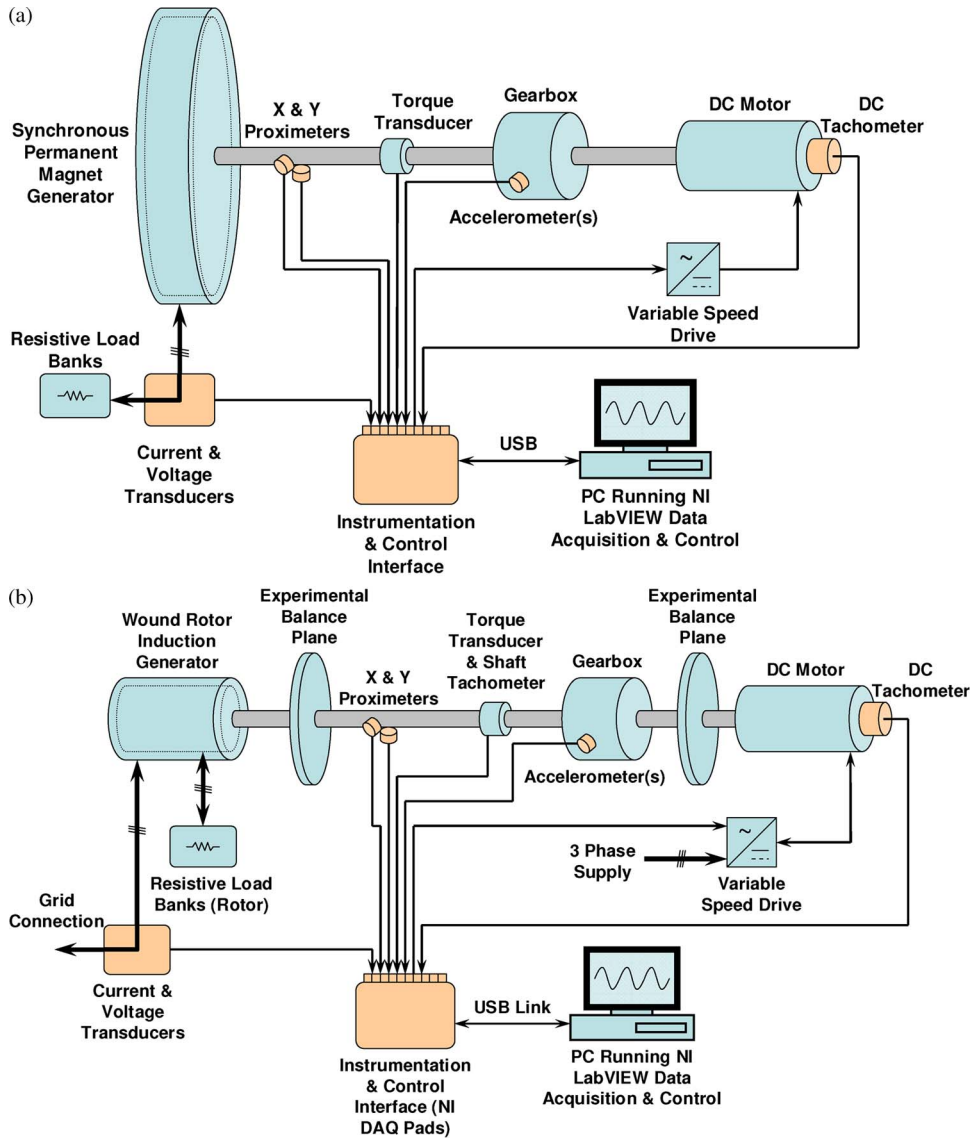


Fig. 6. Schematic diagrams of the WT drive train test rig. (a) With permanent-magnet synchronous generator installed. (b) With induction generator installed.

316 A. WT Drive Train Test Rig

317 One of the difficulties in gaining practical industry experi-
 318 ence of condition monitoring on real WTs is the lack of collab-
 319 oration needed with WT operators and manufacturers, due to
 320 data confidentiality, particularly when faults are present. This
 321 can be avoided by gaining condition monitoring experience
 322 using a controllable experimental test rig to which defined faults
 323 can be applied. Therefore, the technique proposed in this paper
 324 has been validated experimentally on a WT drive train test
 325 rig designed to investigate condition monitoring signals in the
 326 laboratory. This test rig was described in detail in [16] and was
 327 equipped first with a permanent-magnet synchronous generator
 328 and, subsequently, with an induction generator, both as shown
 329 in Fig. 6.

330 The synchronous generator [Fig. 6(a)], such as might be used
 331 in a direct-drive WT, was rated for the experiment at 10 kW,
 332 three-phase 54-pole permanent-magnet machine with a rectified
 333 output feeding a resistive load bank.

The induction generator [Fig. 6(b)], such as might be used
 in a geared-drive WT, was rated for the experiment at 30 kW,
 three-phase four-pole wound-rotor machine, with the rotor cir-
 cuit coupled via slip rings to a three-phase resistive load bank,
 so that rotor electrical imbalance could be applied, and the
 generator stator fed the three-phase mains.

The test rig comprises a 54-kW dc variable-speed motor
 and a two-stage gearbox, instrumented and controlled using
 LabVIEW. In the experiments, a variety of wind speed inputs
 could be applied to the test rig via the dc motor, the speed
 of which is controlled by an external model incorporating the
 properties of natural wind at a variety of speeds and turbulences
 and the mechanical behavior of a 2-MW WT operating under
 closed-loop conditions. Relevant signals were collected from
 the terminals of the generator and the drive train when subjected
 to this driving speed.

A number of electrical and mechanical drive train faults
 could be applied to the test rig. Because they are not necessarily

AQ8

AQ7

precise replicas of WT faults, they have been called “fault-like perturbations” but contain similarities with faults on real WTs. In this paper, to verify the efficacy of the proposed condition monitoring technique for WTs, two “faultlike perturbations” were applied to two different generator configurations as follows.

- 1) In the first configuration, with the synchronous generator representing a direct-drive WT, the “faultlike perturbation” applied was mechanically unbalanced on the generator rotor, representing the effect of a mechanical unbalance fault on the WT generator drive train.
- 2) In the second configuration, with the slip-ring induction generator representing a geared-drive WT, the “fault-like perturbation” applied was electrically asymmetric on the generator rotor, representing the effect of a rotor winding fault, brush imbalance, or air gap eccentricity in the WT generator.

Details of both experimental arrangements are described as follows.

B. Mechanical Unbalance Fault Simulated on Rotor of Synchronous Generator

The mechanical unbalance fault was simulated by attaching a 1-kg mass to the generator rotor with an equivalent rotating mass of 290.7 kg, which is $\sim 0.3\%$. This represents a balance quality grade of $G 7.8$ (7.8 mm/s), within the limit of $G 16$ (16 mm/s) prescribed in ISO1940-1:2003 for a low-speed propeller shaft, applicable to a direct-drive WT shaft. The details of this estimation are given in Appendix A. The peak-to-peak measured displacement of the generator shaft changed a little before and after the placement of the unbalanced mass, varying in the range 90–140 μm . The equivalent vibration velocity would have been 0.13–0.21 mm/s, with the generator running at the maximum rotational speed of 28 r/min well within the 0.71-mm/s limit that is acceptable for machines ≤ 15 kW prescribed in ISO2372:1974.

When the synchronous generator ran at varying speed representing the wind driving situation, the speed, torque, and total power were measured using a sampling frequency of 1 kHz, and the “fault-like perturbation” was periodically applied to the rotor. The time waveforms of the signals before and after the application are shown in Fig. 7(a).

From Fig. 7(a), it can be seen that, in the presence of the mass unbalance fault, the driving shaft torque signal gave a response at the shaft rotational frequency f_{rm} , as expected, fluctuating by 8% range due to the combined effects of mass unbalance fault and wind driving turbulence, which can be compared to fluctuating by 4% due to the wind driving turbulence alone. By contrast, the generator power showed only a slight change in the presence of the fault. In this case, the fault-related frequency is f_{rm} , and the CWT-based energy tracking technique was applied to extract energy at this frequency, as shown in Fig. 7(b). This provided a clear indication of the presence or absence of the mechanical unbalance fault despite the fact that the shaft speed was varying continuously throughout the experiment and the effect could not be observed in the unprocessed total power signal shown in Fig. 7(a).

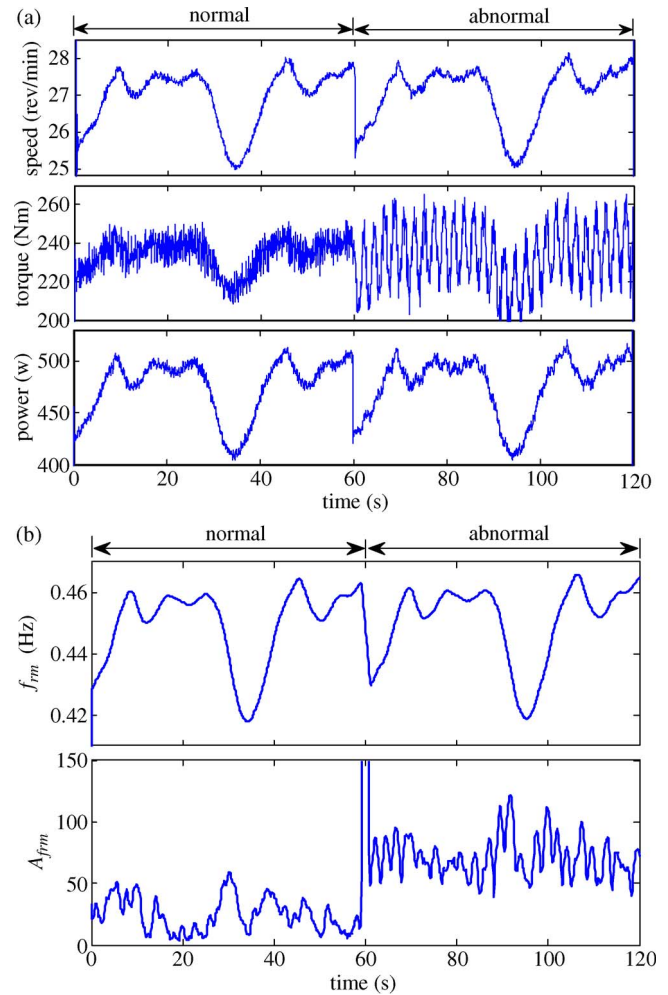


Fig. 7. Mass unbalance fault applied to a synchronous generator rotor on the WT test rig, representing a direct-drive WT. (a) Signals when a mass unbalance fault was simulated on a synchronous generator rotor. (b) Detecting a mass unbalance fault from the power signal.

TABLE II
PARAMETERS USED FOR CALCULATION RESULTS IN FIG. 7

ω_c	ω_f	T
ω_{rm}	$0.03 \omega_{rm}$	$0.2s$

It can be seen from Fig. 7(b) that a 0.3% or $G 7.8$ unbalance fault was easily detectable. This shows that the proposed technique has the potential to detect an incipient mechanical unbalance fault of 0.3% or $G 7.8$ on a direct-drive WT. The parameters used for this calculation are given in Table II.

C. Electrical Asymmetry on Rotor of Induction Generator

The electrical asymmetry was simulated on the induction generator by adjusting the phase resistances in the load bank externally connected to the rotor. Two levels of rotor asymmetry were applied to investigate the effect of an incipient fault. These were an electrical asymmetry of $U_e = 4.7\%$ and, then, a larger asymmetry of 9.2%. The details of the rotor circuit and the estimation of asymmetry are described in Appendix B and in Table IV.

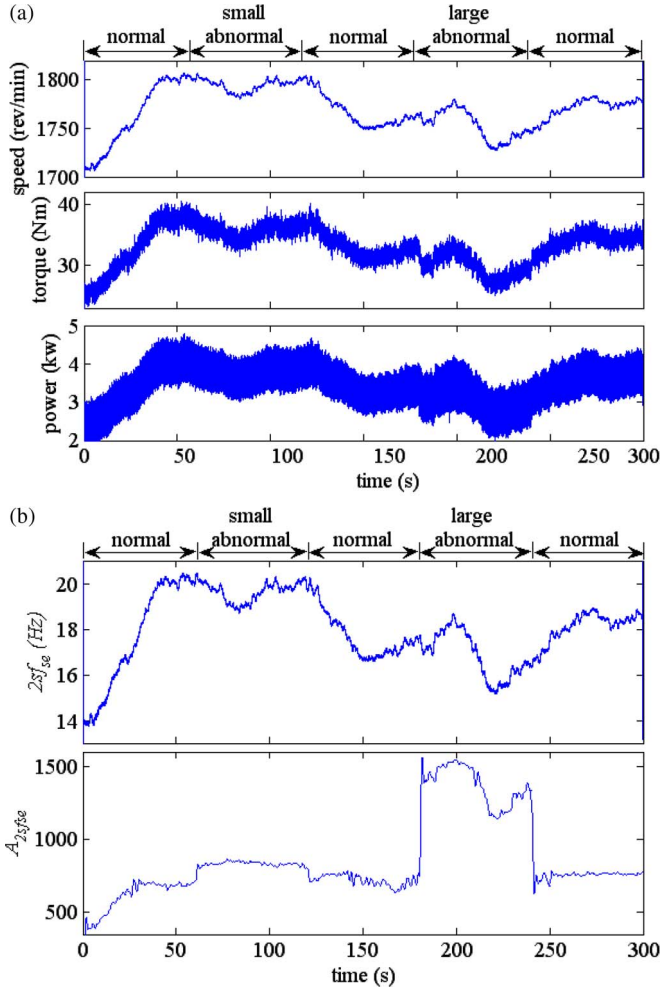


Fig. 8. Electrical asymmetry applied to an induction generator rotor on the test rig, representing a geared-drive WT. (a) Signals when an electrical asymmetry fault was simulated on an induction generator rotor. (b) Detecting an electrical asymmetry fault from the power signal.

As in the mechanical unbalance experiment, the rotational speed, mechanical drive shaft torque, and generator total power signals were measured when the “faultlike perturbation” was periodically applied to the rotor. A smaller fault was applied in the period 60–120 s and a larger fault between 180 and 240 s, with the rotor circuits being balanced in the periods 0–60 s, 120–180 s, and 240–300 s. The time waveforms of the signals collected in this experiment are shown in Fig. 8(a), and it can be seen that, due to the effect of the varying generator speed, the fault symptom cannot be observed clearly from either the generator shaft torque or total power.

When the rotor phase resistances are imbalanced, the generator current, voltage, and power are modulated twice by the slip frequency as the rotor asymmetry moves through the air gap magnetic field twice for every pole pair cycle [4]. Therefore, in this case, the fault-related frequency is $2sf_{se}$, and the CWT-based energy tracking technique was applied to extract the energy at that frequency, as shown in Fig. 8(b).

From Fig. 8(b), it can be seen that the smaller, 4.7%, fault was not clear although it is still visible, so the condition monitoring algorithm had limited detectability in this case. This lack of detectability was due to the residual imbalances present in the

TABLE III
PARAMETERS USED FOR CALCULATION RESULTS IN FIG. 8

ω_c	ω_f	T
$2sf_{se}$	$0.4sf_{se}$	$0.12s$

rotor windings, brush gear, and connections, as well as the negative influence of the timely varying generator rotational speed which partially hid the faulty feature. However, the larger 9.2% fault was clearly visible in the figure and, therefore, readily detectable despite the fact that the $2sf_{se}$ frequency signal was varying during the experimental processes.

This shows that the proposed technique has the potential to detect an incipient 9.2% electrical asymmetry fault on a geared-drive WT generator. The parameters used for this calculation are given in Table III.

V. CONCLUSION

To improve the WT availability and reduce the O&M costs, a new WT condition monitoring technique has been proposed. From this research, the following conclusions can be reached.

- In comparison with the conventional vibration, temperature measurement, and lubrication oil analysis, the technique proposed shows the following potential advantages:
 - reduced capital cost;
 - ability to detect both electrical and mechanical faults;
 - applicable to both geared and direct-drive WTs.
- The proposed CWT-based energy tracking method not only reduces the calculation needed to extract features from lengthy online data but also provides a feasible condition monitoring approach that is applicable to WTs operating at either fixed or variable speed.
- Experiments have shown that the proposed technique is capable of detecting both mechanical and electrical faults in WT drive trains of different types.
- The technique is a feasible way to establish a simple, cheap, but potentially global cost-effective CMS for a WT.

The technique now needs to be applied to the power signals obtained from real WTs during real mechanical and electrical faults to determine the detectability of the algorithm and its ability to detect incipient faults in both cases.

Further work will also be needed to establish the ability of this technique for a wider range of faults and for a variable-speed WT under closed-loop control.

APPENDIX A GENERATOR ROTOR MECHANICAL UNBALANCE

Based on BS ISO1940-1:2003, the balance quality grade G may be calculated by

$$G = e \cdot 2\pi f_{rm} \quad (A1)$$

where

$$e = mr/M_{eq} \quad (A2)$$

$$U_m = (m/M_{eq}) \times 100. \quad (A3)$$

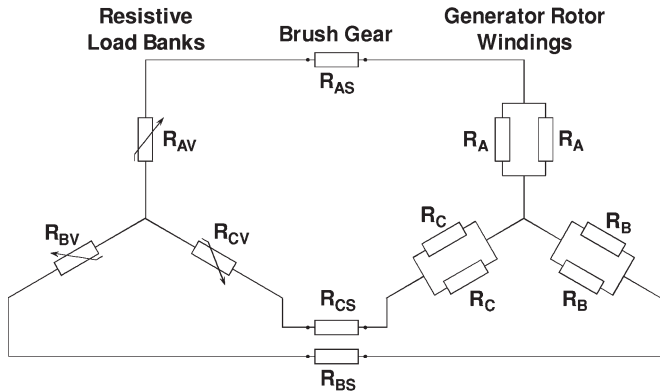


Fig. 9. Rotor circuit diagram, including a resistive load bank.

TABLE IV
ELECTRICAL ASYMMETRY APPLIED TO TEST RIG IN FIG. 8

Time (s)	Description	U_e (%)
0 – 60s	Balanced	0.0
60 – 120s	Low asymmetry	4.7
120 – 180s	Balanced	0.0
180 – 240s	High asymmetry	9.2
240 – 300s	Balanced	0.0

489 For the test rig shown in Fig. 6(a), the unbalance mass $m =$
490 1.0 kg, the effective radius $r = 865$ mm, and the equivalent
491 rotating mass of the test rig $M_{eq} = 290.7$ kg. The average
492 rotational speed of the generator rotor is 25 r/min. This gives
493 a balance quality grade and mechanical unbalance for Fig. 7 of
494 $G 7.8$ ($G = 7.8$ mm/s) and $U_m = 0.3\%$, respectively.

APPENDIX B

GENERATOR ROTOR ELECTRICAL ASYMMETRY

497 The details of the generator rotor circuit shown in Fig. 6(b)
498 taking into account the external resistive load bank are shown
499 in Fig. 9.

500 The balanced circuit resistances were given by

$$\begin{cases} R_{AB} = R_{AV} + R_{BV} + R_{AS} + R_{BS} + (R_A + R_B)/2 \\ R_{BC} = R_{BV} + R_{CV} + R_{BS} + R_{CS} + (R_B + R_C)/2 \\ R_{CA} = R_{CV} + R_{AV} + R_{CS} + R_{AS} + (R_C + R_A)/2. \end{cases} \quad (\text{B1})$$

501 The circuits are balanced, giving

$$R_{AB} = R_{BC} = R_{CA} = \bar{R} = 7.60 \Omega \quad (\text{B2})$$

AQ10 502 where $\bar{R} = (R_{AB} + R_{BC} + R_{CA})/3$.

503 Then, the electrical imbalance can be estimated through
504 calculating the residual circuit resistance δR , i.e.,

$$\delta R = |R_{AB}e^{i\theta_1} + R_{BC}e^{i\theta_2} + R_{CA}e^{i\theta_3}| \quad (\text{B3})$$

505 where $i = \sqrt{-1}$, $\theta_1 = 0$, $\theta_2 = 2\pi/3$, and $\theta_3 = 4\pi/3$.

506 The percentage fault can be described by

$$U_e = (\delta R / \bar{R}) \times 100. \quad (\text{B4})$$

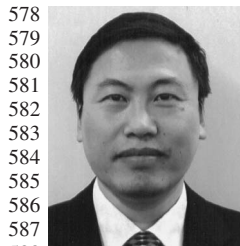
The larger the value of U_e , the more serious the electrical
507 asymmetry. The electrical asymmetries applied in Fig. 8 are
508 listed in Table IV. 509

ACKNOWLEDGMENT

The authors would like to thank the New and Renewable En-
511 ergy Centre, Blyth, for the assistance for the original provision
512 of the test rig. 513

REFERENCES

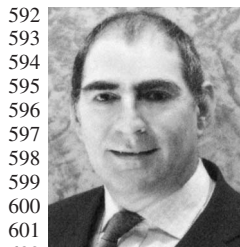
- [1] J. F. Manwell, A. L. Rogers, and J. G. McGowan, "Status of offshore wind
515 energy in the United States," in *Proc. IEEE Power Eng. Soc. Summer*
516 *Meeting*, Jul. 15–19, 2001, vol. 1, pp. 10–13. 517
- [2] H. Polinder, F. F. A. van der Pijl, G. J. de Vilder, and P. J. Tavner, "Com-
518 parison of direct-drive and geared generator concepts for wind turbines,"
519 *IEEE Trans. Energy Convers.*, vol. 21, no. 3, pp. 725–733, Sep. 2006. 520
- [3] J. Nilsson and L. Bertling, "Maintenance management of wind power
521 systems using condition monitoring systems—Life cycle cost analysis for
522 two case studies," *IEEE Trans. Energy Convers.*, vol. 22, no. 1, pp. 223–
523 229, Mar. 2007. 524
- [4] P. J. Tavner, "Review of condition monitoring of rotating electrical ma-
525 chines," *IET Elect. Power Appl.*, vol. 2, no. 4, pp. 215–247, Jul. 2008. 526
- [5] D. Casadei, F. Filippetti, A. Yazidi, C. Rossi, and G. A. Capolino, "Diag-
527 nostic technique based on rotor modulating signals signature analysis for
528 doubly fed induction machines in wind generator systems," in *Conf. Rec.*
529 *IEEE IAS Annu. Meeting*, Oct. 8–12, 2006, vol. 3, pp. 1525–1532. 530
- [6] A. Bellini, F. Filippetti, C. Tassoni, and G. A. Capolino, "Advances in di-
531 agnostic techniques for induction machines," *IEEE Trans. Ind. Electron.*,
532 vol. 55, no. 12, pp. 4109–4126, Dec. 2008. 533
- [7] P. Caselitz and J. Giehardt, "Rotor condition monitoring for improved
534 operational safety of offshore wind energy converters," *Trans. ASME, J.*
535 *Sol. Energy Eng.*, vol. 127, no. 2, pp. 253–261, May 2005. 536
- [8] F. Spinato, P. J. Tavner, G. J. W. van Bussel, and E. Koutoulakos, "Reli-
537 ability of wind turbine subassemblies," *IET Renew. Power Gener.*, vol. 3,
538 no. 4, pp. 1–15, 2009. 539
- [9] S. F. Legowski, A. H. M. Sadrul Ula, and A. M. Trzynadlowski, "Instanta-
540 neous power as a medium for the signature analysis of induction motors,"
541 *IEEE Trans. Ind. Appl.*, vol. 32, no. 4, pp. 904–909, Jul./Aug. 1996. 542
- [10] W. Q. Jeffries, J. A. Chambers, and D. G. Infield, "Experience with
543 bicoherence of electrical power for condition monitoring of wind turbine
544 blades," *Proc. Inst. Elect. Eng.—Vis. Image Signal Process.*, vol. 145,
545 no. 3, pp. 141–148, Jun. 1998. 546
- [11] W. Yang, P. J. Tavner, C. J. Crabtree, and M. Wilkinson, "Research on a
547 simple, cheap but globally effective condition monitoring technique for
548 wind turbines," presented at the XVIII Int. Conf. Electrical Machines
549 (ICEM), Vilamoura, Portugal, Sep., 2008, Paper ID 1053. 550
- [12] J. Cusido, L. Romeral, J. A. Ortega, J. A. Rosero, and A. E. Garcia, "Fault
551 detection in induction machines using power spectral density in wavelet
552 decomposition," *IEEE Trans. Ind. Electron.*, vol. 55, no. 2, pp. 633–643,
553 Feb. 2008. 554
- [13] A. Ordaz-Moreno, R. de Jesus Romero-Troncoso, J. A. Vite-Frias,
555 J. R. Rivera-Gillen, and A. Garcia-Perez, "Automatic online diagnosis
556 algorithm for broken-bar detection on induction motors based on discrete
557 wavelet transform for FPGA implementation," *IEEE Trans. Ind. Electron.*,
558 vol. 55, no. 5, pp. 2193–2202, May 2008. 559
- [14] M. Riera-Guasp, J. A. Antonino-Daviu, M. Pineda-Sanchez,
560 R. Puche-Panadero, and J. Perez-Cruz, "A general approach for the
561 transient detection of slip-dependent fault components based on the
562 discrete wavelet transform," *IEEE Trans. Ind. Electron.*, vol. 55, no. 12,
563 pp. 4167–4180, Dec. 2008. 564
- [15] S. S. Tsai, C. T. Hsieh, and S. J. Huang, "Enhancement of damage-
565 detection of wind turbine blades via CWT-based approaches," *IEEE*
566 *Trans. Energy Convers.*, vol. 21, no. 3, pp. 776–781, Sep. 2006. 567
- [16] W. Yang, P. J. Tavner, and M. Wilkinson, "Condition monitoring and
568 fault diagnosis of a wind turbine synchronous generator drive train," *IET*
569 *Renew. Power Gener.*, vol. 3, no. 1, pp. 1–11, Mar. 2009. 570
- [17] E. Wiggelinkhuizen, T. Verbruggen, H. Braam, L. Rademakers, J. Xiang,
571 and S. Watson, "Assessment of condition monitoring techniques for off-
572 shore wind farms," *Trans. ASME, J. Sol. Energy Eng.*, vol. 130, no. 3,
573 pp. 1–9, Aug. 2008. 574
- [18] S. K. Lee, "An acoustic decay measurement based on time–frequency
575 analysis using wavelet transform," *J. Sound Vib.*, vol. 252, no. 1, pp. 141–
576 153, Apr. 2002. 577



Wenxian Yang received the Ph.D. degree in mechanical engineering from Xi'an Jiaotong University, Xi'an, China, in 1999. He completed his postdoctoral research in Northwestern Polytechnical University, Xi'an, in 2001.

He was with the City University of Hong Kong, Kowloon, Hong Kong; Nottingham Trent University, Nottingham, U.K.; Cranfield University, Cranfield, U.K.; and Durham University, Durham, U.K. He is currently a Technical Specialist with the New and Renewable Energy Centre, Blyth, U.K. He has

worked in the areas of new and renewable energy, signal processing, machine condition monitoring and fault diagnosis, nondestructive testing and nondestructive evaluation, and artificial intelligence in both industry and academia.



Peter J. Tavner (SM'08) received the M.A. degree from Cambridge, U.K., in 1969 and the Ph.D. degree from Southampton, U.K., in 1978.

He held research and technical positions in the industry, including Group Technical Director with FKI Energy Technology, Loughborough, U.K. He is currently the Head of the School of Engineering and Computing Sciences, Durham University, Durham, U.K., and a Professor with the New and Renewable Energy Centre, Blyth, U.K. His research interest includes machines for renewable energy, condition

monitoring, and reliability. Dr. Tavner was the recipient of the Institution Premium of the Institution of Electrical Engineers, U.K.



Christopher J. Crabtree received the M.S. degree in engineering from Durham University, Durham, U.K., in 2007 having studied new and renewable energy as an electrical engineer, where he is currently working toward the Ph.D. degree in condition monitoring of offshore wind turbines.

His research interests include the development of condition monitoring techniques using industrial data and a test rig.

AQ16

606

607

608

609

610

611

612

613

614



Michael Wilkinson received the M.Sc. degree in electromagnetic sensing from Durham University, Durham, U.K., in 2003 and the Eng.D. degree with a thesis on condition monitoring for offshore wind turbines from Newcastle University, Newcastle upon Tyne, U.K., in 2007, in a collaborative project with Durham University and FKI Energy Technology.

In 2007, he joined Garrad Hassan, Bristol, U.K., as part of the operational projects team, where he has been monitoring wind farms worldwide on behalf of owners. His research interests include condition monitoring and reliability of wind turbines.

AQ17

615

616

617

618

619

620

621

622

623

624

625

626

AUTHOR QUERIES

AUTHOR PLEASE ANSWER ALL QUERIES

- AQ1 = “EPSRC” was defined as “Engineering and Physical Sciences Research Council.” Please check if appropriate.
- AQ2 = Current affiliation was provided in the first footnote for author Wenxian Yang to be consistent with the current affiliation in the vitae. Please check if appropriate.
- AQ3 = Current affiliation was provided in the first footnote for author Peter J. Tavner to be consistent with the current affiliation in the vitae. Please check if appropriate.
- AQ4 = Current affiliation was provided in the first footnote for author Christopher J. Crabtree to be consistent with the current affiliation in the vitae. Please check if appropriate.
- AQ5 = Current affiliation was provided in the first footnote for author Michael Wilkinson to be consistent with the current affiliation in the vitae. Please check if appropriate.
- AQ6 = Please check if call-out a) in upper left corner of Fig. 1 should be deleted.
- AQ7 = Please check on the edits for this sentence if it is appropriate. Originally, the sentence was “The synchronous generator, Fig. 6(a), was such as might be used in a direct drive WT, rated for the experiment at 10 kW, 3-phase, 54-pole, permanent-magnet machine with a rectified output feeding a resistive load bank.”
- AQ8 = Please check on the edits for this sentence if appropriate.
- AQ9 = “rev/min” was changed to “r/min” for revolution per minute to follow IEEE style. Please check if appropriate.
- AQ10 = “Ohm” was changed to symbol “ Ω .” Please check if appropriate.
- AQ11 = “NDT” was defined as “nondestructive testing.” Please check if appropriate.
- AQ12 = “NDE” was defined as “nondestructive evaluation.” Please check if appropriate.
- AQ13 = Please provide academic institution for the M.A. degree received.
- AQ14 = Please provide academic institution for the Ph.D. degree received.
- AQ15 = “Centre” was added after “New and Renewable Energy,” and address was provided for the center. Please check if appropriate.
- AQ16 = “Masters in Engineering” was changed to “M.S. degree in engineering.” Please check if appropriate.
- AQ17 = Please check if the provided address for Garrad Hassan is correct.

END OF ALL QUERIES

Cost-Effective Condition Monitoring for Wind Turbines

Wenxian Yang, Peter J. Tavner, *Senior Member, IEEE*, Christopher J. Crabtree, and Michael Wilkinson

Abstract—Cost-effective wind turbine (WT) condition monitoring assumes more importance as turbine sizes increase and they are placed in more remote locations, for example, offshore. Conventional condition monitoring techniques, such as vibration, lubrication oil, and generator current signal analysis, require the deployment of a variety of sensors and computationally intensive analysis techniques. This paper describes a WT condition monitoring technique that uses the generator output power and rotational speed to derive a fault detection signal. The detection algorithm uses a continuous-wavelet-transform-based adaptive filter to track the energy in the prescribed time-varying fault-related frequency bands in the power signal. The central frequency of the filter is controlled by the generator speed, and the filter bandwidth is adapted to the speed fluctuation. Using this technique, fault features can be extracted, with low calculation times, from direct- or indirect-drive fixed- or variable-speed WTs. The proposed technique has been validated experimentally on a WT drive train test rig. A synchronous or induction generator was successively installed on the test rig, and both mechanical and electrical fault-like perturbations were successfully detected when applied to the test rig.

Index Terms—Adaptive signal processing, condition monitoring, fault diagnosis, induction generators, signal processing, synchronous generators, time-frequency analysis, wavelet transforms, wind power generation.

NOMENCLATURE

A	Estimated energy of the frequency component of interest.
a_{\min}, a_{\max}	Minimum and maximum wavelet scales considered by the adaptive bandpass filter.
a	Wavelet scale.
b	Wavelet time-shift parameter.
ε	Voltage or current transducer error.
e	Specific unbalance.
f_{rm}	Rotational frequency of the generator rotor.
f_{se}	Electrical supply frequency.

G	Balance quality grade.	41
I_i	Line currents.	42
m	Unbalanced mass.	43
M_{eq}	Equivalent mass of the test rig rotor.	44
ω	Angular frequency of interest.	45
ω_c	Mean frequency of the prescribed frequency component during the time interval T .	46–47
ω_{fg}	Fluctuation of the generator rotational frequency.	48–49
ω_f	Fluctuation of the frequency of interest.	50–51
$\omega_{upper}, \omega_{lower}$	Upper and lower cutoff frequencies of the adaptive filter.	52–53
ω_0	Central angular frequency of the mother wavelet.	54–55
ω_{rm}	Angular rotational frequency of the generator rotor.	56–57
P	Three-phase total power output from the generator.	58–59
r	Effective radius of the equivalent unbalanced mass.	60–61
R_{AB}, R_{BC}, R_{CA}	Combined line-to-line resistances.	62
R_{AS}, R_{BS}, R_{CS}	Brush gear and slip ring resistances.	63
R_{AV}, R_{BV}, R_{CV}	Load bank resistances.	64
R_A, R_B, R_C	Generator rotor winding resistances.	65
δR	Electrical resistance imbalance.	66
s	Induction machine slip.	67
ψ	Mother wavelet function.	68
T	Sliding window averaging time interval.	69
t_0	Starting time moment of the sliding window.	70–71
U_e	Electrical asymmetry on the generator rotor.	72–73
U_m	Mechanical unbalance on the generator rotor.	74–75
V_i	Phase voltages.	76
x	Real-time signal.	77
η	Constant between ω_{fg} and ω_f .	78

Manuscript received December 5, 2008; revised September 3, 2009. This work was supported by the U.K. Engineering and Physical Sciences Research Council Supergen Wind Program EP/D034566/1.

W. Yang is with the New and Renewable Energy Centre, NE24 3AG Blyth, U.K.

P. J. Tavner is with the School of Engineering and Computing Sciences, Durham University, DH1 3LE Durham, U.K., and also with the New and Renewable Energy Centre, NE24 3AG Blyth, U.K. (e-mail: Peter.Tavner@durham.ac.uk).

C. J. Crabtree is with Durham University, DH1 3LE Durham, U.K.

M. Wilkinson is with Garrad Hassan, BS2 0QD Bristol, U.K.

Color versions of one or more of the figures in this paper are available online at <http://ieeexplore.ieee.org>.

Digital Object Identifier 10.1109/TIE.2009.2032202

I. INTRODUCTION 79

OVER THE last 40 years, there has been an increased application of wind turbines (WTs) around the world, 81 with growth in rating from 30 kW to > 5 MW and, more 82 recently, their application offshore [1]. To reduce the cost of 83 energy from WTs, there is a pressing need to improve the WT 84 availability and reduce the operational and maintenance (O&M) 85

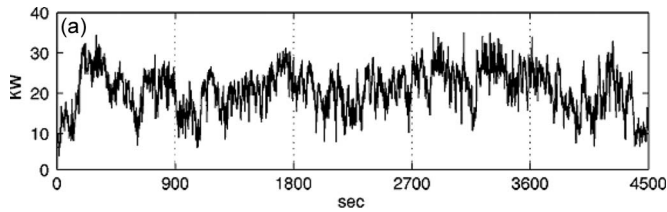


Fig. 1. Variation in power output from a 33-kW fixed-speed WT over five successive periods of 900 s, each showing the large variation in the signal due to wind turbulence (taken from [7]).

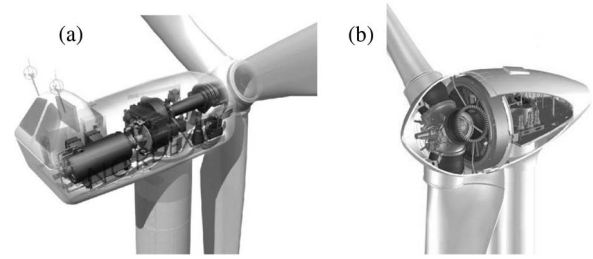


Fig. 2. Structures of real large WTs. (a) Geared. (b) Direct drive.

86 costs. Aside from developing more advanced machine designs
87 [2] to improve the availability, an effective way to achieve
88 this improvement would be to apply reliable and cost-effective
89 condition monitoring [3], which is why this subject is attracting
90 industrial and academic attention.

91 The wind industry currently uses condition monitoring sys-
92 tems (CMSs), such as vibration, temperature, lubrication oil,
93 and generator current analysis, developed from other rotating
94 machine power generation industries [4]–[6], where they have
95 achieved success. However, despite their application in the
96 wind industry [7], they have not yet proven their effectiveness
97 due to the peculiarities of a WT, which has a slow speed and
98 rapidly varying torque. Commercial WT CMSs mostly employ
99 vibration-based techniques, which are sophisticated, and the
100 sensors and cabling are costly. The technique is also not ideally
101 suited to all WT types and faults. Lubrication oil analysis is
102 becoming more popular for detecting gearbox tooth and bearing
103 wear but cannot detect failures outside the gearbox. More
104 advanced techniques, such as optical strain measurement, have
105 been developed for monitoring WT blade integrity. However,
106 these are expensive, and recent reliability surveys [8] have
107 shown that WT electrical systems have a higher failure rate than
108 the mechanical systems. For these reasons, an electrically based
109 WT CMS would be beneficial and could be more compre-
110 hensive, simpler, and cheaper than other techniques. This paper will
111 propose such a technique.

112 Instantaneous electric power measurement has been demon-
113 strated on induction machines for detecting motor faults [9].
114 Three-phase total power monitoring has also been applied to
115 WTs as a condition monitoring and fault diagnosis signal [10]
116 but has not achieved commercial application. This research will
117 be based entirely on the use of this signal and the generator
118 speed for condition monitoring. Power output measurement
119 was considered for condition monitoring in [7] and [10], but
120 Fig. 1, taken from [7], shows how the WT power output signal
121 experiences continuous and rapid variations during operation.

122 The work reported in this paper is an enhancement of the
123 research described in [11], now including the following:

- 124 1) a more comprehensive description of the background
125 technology and the state of the art of the proposed
126 technique;
- 127 2) an improved mathematical presentation;
- 128 3) additional figures to enhance the description of the
129 technique;
- 130 4) more substantial experimental results;
- 131 5) an amended conclusion.

The novelties of the proposed technique are summarized as 132
follows: 133

- 1) a technique for WT condition monitoring based on mea- 134
suring the generator total power signal rather than more 135
conventional measurements validated by experiments on 136
a test rig with a simple fault setup; 137
- 2) a new adaptive continuous-wavelet-transform (CWT)- 138
based energy tracking method, reducing the calculation 139
time for feature extraction when applied to lengthy sig- 140
nals, making possible less time-intensive WT condition 141
monitoring; 142
- 3) the successful detection of two types of fault using this 143
method has been demonstrated on two WT arrangements, 144
including both electrical and mechanical faults; 145
- 4) the proposed method is more efficient for the detection 146
of faults in variable-speed WTs than other more conven- 147
tional techniques; 148
- 5) the technique used in this paper can be applied to any WT 149
generator for tracking any characteristic, fault-related fre- 150
quency component, so it is general and could be applied 151
to detect a variety of faults depending on the choice of 152
frequency selected. 153

Wavelet transforms have been successfully used in condition 154
monitoring and diagnosis of rotating electrical machine faults 155
[1], [12]–[14]. However, most used the discrete wavelet trans- 156
form (DWT) rather than the CWT, although the latter is superior 157
to the former in multiresolution signal analysis. However, the 158
CWT involves more intensive convolution calculations than the 159
DWT, making it more difficult to process lengthy online data, 160
such as WT monitoring signals. Moreover, it is inconvenient to 161
apply the traditional time–frequency–amplitude CWT image to 162
machine condition monitoring, as was done in [15]. Wavelets 163
have been proposed for WT condition monitoring [16], [17] but 164
have not yet received commercial application. 165

II. APPLYING GENERATOR POWER MONITORING TO WTs 166

A WT converts the kinetic energy of the wind into electrical 167
energy, utilizing mechanical and electrical conversion, control, 168
and transmission systems. The architectures of two commonly 169
used large WTs are shown in Fig. 2. 170

The application of vibration, temperature, and lubrication oil 171
techniques to monitoring WTs should improve their availability 172
but, to date, is not being widely used for the following reasons: 173

- 1) lack of practical industry experience with condition mon- 174
itoring in the wind environment; 175
- 2) difficulties collecting and interpreting the data, including 176
the risk of false or missed alarms; 177

178 3) the fact that present techniques may not be suited to all
 179 types of WTs such as shown in Fig. 2;
 180 4) the fact that developing reliable WT condition monitoring
 181 techniques requires complex and lengthy collaboration
 182 between WT operators and manufacturers in the field.

183 WT power flows are disturbed by both mechanical and
 184 electrical faults [16], [17]. To measure the WT shaft torque is
 185 costly and usually impractical for a real WT. In contrast, shaft
 186 speed and electrical power output are routinely monitored for
 187 WTs, but, to date, commercial CMSs do not use these signals.
 188 In comparison with conventional stator current analysis,
 189 widely adopted for condition monitoring motors [4], [6], power
 190 monitoring could have the following disadvantages.

191 1) The error in the total power signal depends not only on
 192 the voltage and current transducer error ε but also on the
 193 measurement method. In the three-wattmeter method, the
 194 error will be 6ε , but, in the two-wattmeter method,
 195 the error is limited to 4ε , whereas the current signal error
 196 would be only ε . Therefore, the signal-to-noise ratio for
 197 basic analysis should be better for current than power
 198 analysis.

199 On the other hand, monitoring based on power analysis could
 200 have the following advantages.

201 1) The power signal is already available from the generator
 202 terminal voltage and current signals for the control of the
 203 WT and can conveniently be accessed.
 204 2) Fewer cheaper transducers than accelerometers and oil
 205 debris probes are required for power monitoring.
 206 3) Mechanical and electrical faults both disturb the genera-
 207 tor power output, so power monitoring could detect both
 208 types of faults.
 209 4) Single line current analysis contains the mains frequency
 210 carrier, whereas this is absent in the power signal. There-
 211 fore, the signal-to-noise ratio for faulty feature analysis
 212 should be better for power than current analysis, balanc-
 213 ing the aforementioned transducer error effect.
 214 5) In the power signal, the fault-related frequency side-
 215 bands, around the mains frequency, are folded down
 216 around dc, limiting the bandwidth needed to monitor the
 217 signal.

218 An example of the current, voltage, and power signals mea-
 219 sured under faulty conditions on an induction generator, fitted to
 220 the test rig described in the following, is shown in Fig. 3, where
 221 the signals were collected when a periodic rotor electrical
 222 asymmetry was applied in the presence of serious noise due
 223 to power system imbalance.

224 The fault in Fig. 3 was applied at the time intervals of 20–40 s
 225 and 60–80 s and was absent in the other time intervals. It
 226 can be seen that the amplitudes of both the current–time and
 227 voltage–time waveforms gave no indication of abnormal con-
 228 ditions, whereas the total three-phase power signal P changes
 229 significantly during the abnormality due to the presence of $2f_{se}$
 230 and $2sf_{se}$ components. The total power $P(t)$ was calculated
 231 using

$$P(t) = \sum_{i=1}^3 I_i(t) \cdot V_i(t). \quad (1)$$

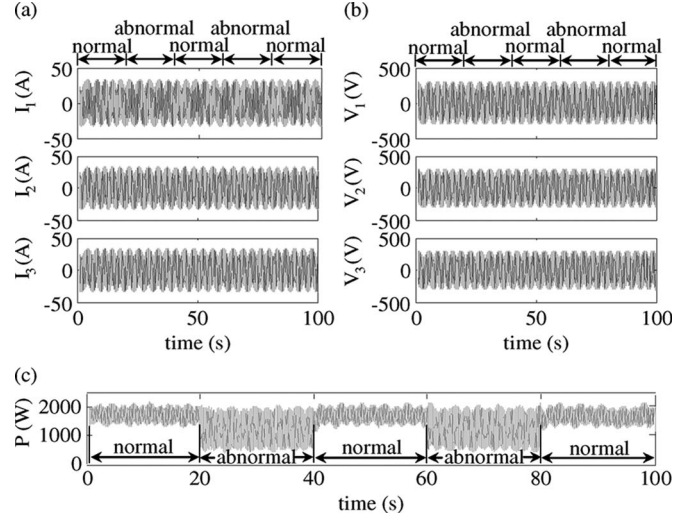


Fig. 3. Comparison of current, voltage, and total power signal in the presence of a rotor asymmetry fault. (a) Line currents. (b) Phase voltages. (c) Total power.

III. DESIGN OF WAVELET-BASED ADAPTIVE FILTER 232

In this paper, a CWT-based adaptive filter has been designed 233
 to track the energy in the power signal in the prescribed fault- 234
 related frequency bands rather than at all frequencies of the 235
 monitoring signal. In this way, the wavelet calculation can 236
 significantly be reduced, and the results can be displayed graph- 237
 ically rather than as a screen dump image, making the technique 238
 attractive for online application. Details of the technique are 239
 described as follows. 240

The CWT of a real-time signal $x(t)$ can be defined as 241

$$\text{CWT}(b, a) = \frac{1}{\sqrt{|a|}} \int_{-\infty}^{\infty} x(t) \psi^* \left(\frac{t-b}{a} \right) dt \quad (2)$$

where the asterisk “*” indicates the complex conjugate. 242

Traditionally, the wavelet function $\psi(t)$ is dilated or com- 243
 pressed by changing the scale parameter a so that all signal 244
 components ranging from frequency 0 to half the sampling 245
 frequency can be projected onto an appropriate time-scale map, 246
 as shown in Fig. 4. The bottom figure shows the time waveform 247
 of a sample signal of increasing frequency being inspected; the 248
 top figure shows the wavelet coefficients of this signal obtained 249
 at different wavelet scales and times. 250

Many of the calculations shown in Fig. 4 are unnecessary for 251
 WT condition monitoring because the fault-related frequencies 252
 are few in number and the energy extracted at nonfault-related 253
 frequencies is not helpful to assess the machine condition. 254

Therefore, an adaptive CWT-based filter has been designed, 255
 which only extracts energy at known fault frequencies, while 256
 frequencies unrelated to the fault are left unprocessed. The 257
 calculation time for the new technique will be much shorter 258
 than that for a conventional CWT applied to a broad band- 259
 width signal. Therefore, the proposed CWT-based energy 260
 tracking technique should prove more efficient for online 261
 processing of WT monitoring signals than conventional CWT 262
 processing. 263

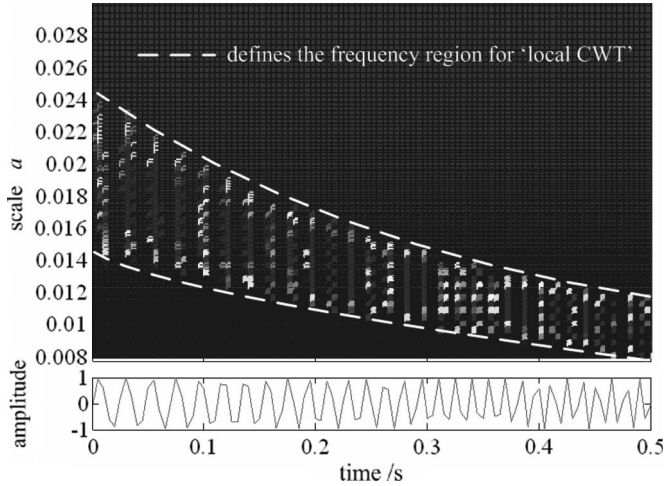


Fig. 4. Illustrative example of the conventional CWT.

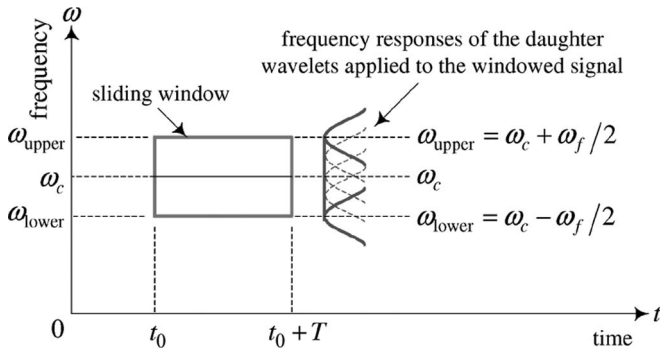


Fig. 5. Two-dimensional sliding window.

264 A time–frequency sliding window has been designed for this
265 task, as shown in Fig. 5. Its central frequency ω_c is the mean
266 frequency during the time interval T of the prescribed fault-
267 related frequency band. The upper and lower cutoff frequencies
268 ω_{upper} and ω_{lower} are adapted to the fluctuation of the generator
269 rotational speed ω_{fg} in that interval, i.e.,

$$\begin{cases} \omega_{\text{upper}} = \omega_c + \omega_f/2 \\ \omega_{\text{lower}} = \omega_c - \omega_f/2 \\ \omega_f = \eta\omega_{\text{fg}}. \end{cases} \quad (3)$$

270 From Fig. 4, it is noticed that ω_f could also be a time-
271 varying parameter, intrinsically dependent on the turbulence of
272 the wind. Experience has shown that onshore wind turbulence
273 varies between 12% and 20%, whereas offshore turbulence
274 approximates to $\sim 6\%$.

275 The relationship between any prescribed frequency ω and its
276 corresponding wavelet scale a is

$$a = \frac{\omega_0}{\omega}. \quad (4)$$

277 With the aid of (3) and (4), the range of the wavelet scales
278 for conducting bandpass filtering can be determined by

$$a \in [a_{\text{min}} \quad a_{\text{max}}] \quad (5)$$

$$\begin{cases} a_{\text{min}} = \frac{\omega_0}{\omega_{\text{upper}}} \\ a_{\text{max}} = \frac{\omega_0}{\omega_{\text{lower}}}. \end{cases} \quad (6)$$

TABLE I
COMPUTATIONAL EFFICIENCY COMPARISON BETWEEN CWT, DWT,
AND PROPOSED APPROACH

Method	Time cost	Operation manner	Accuracy
CWT	18.91s	All frequencies between zero and half sampling frequency are calculated.	Good
DWT	0.31s	Interested frequency band is determined in a rigid dyadic step way.	Not good
Energy tracking	0.16s	Interested frequency band is determined intelligently.	As good as CWT

Subsequently, by performing the CWT locally in the scale 279
range defined by (5), a matrix of wavelet coefficients is obtained 280

$$\text{CWT}_{\text{local}}(b, a) = \frac{1}{\sqrt{|a|}} \int_{-\infty}^{\infty} x(t) \psi^* \left(\frac{t-b}{a} \right) dt. \quad (7)$$

The energy A of the frequency component of interest in the 281
time interval T is estimated by 282

$$A(t_0 + T/2) = \max(|\text{CWT}_{\text{local}}(b, a)|) \quad \begin{cases} a \in [a_{\text{min}} \quad a_{\text{max}}] \\ b \in [t_0 \quad t_0 + T]. \end{cases} \quad (8)$$

The sliding window is moved forward along the signal; the 283
maximum and minimum wavelet scales in (5) being redefined 284
within each time interval according to the generator rotational 285
speed ω_{fg} . Then, using the aforementioned technique, the en- 286
ergy A in the fault-related frequency band is calculated in each 287
time interval using (7) and (8). These calculations are repeated 288
until the whole signal has been processed. Finally, a curve 289
of the energy variation in the fault-related frequency band is 290
obtained, and changes in the running condition of the WT can 291
be assessed. 292

This task could have been accomplished using a series of 293
conventional bandpass filters set up to cover the expected speed 294
range of the turbine. However, such an analysis would not have 295
the advantages of the CWT in processing nonstationary signals 296
shown in Fig. 1 and [18]. 297

To verify the computational efficiency of the proposed tech- 298
nique compared to the traditional CWT and DWT, a calculation 299
was performed to extract the 50-Hz energy component from 300
1 s of line current signal, sampled at a frequency of 2 kHz. 301
The time taken by each approach is listed in Table I. The 302
calculations were done in a computer with 1.4 GHz of Intel 303
Pentium processor and 512 MB of RAM. 304

From Table I, it can be concluded that the proposed energy 305
tracking technique is the most computationally efficient of the 306
three approaches. 307

IV. WT CONDITION MONITORING BY POWER SIGNAL ANALYSIS 308 309

In view of the proposed advantages of generator power 310
signal analysis for detecting both mechanical and electrical 311
faults in a variety of designs of WT drive train, it has been 312
applied in this paper, in combination with the energy tracking 313
method described previously, to develop a new WT condition 314
monitoring technique. 315

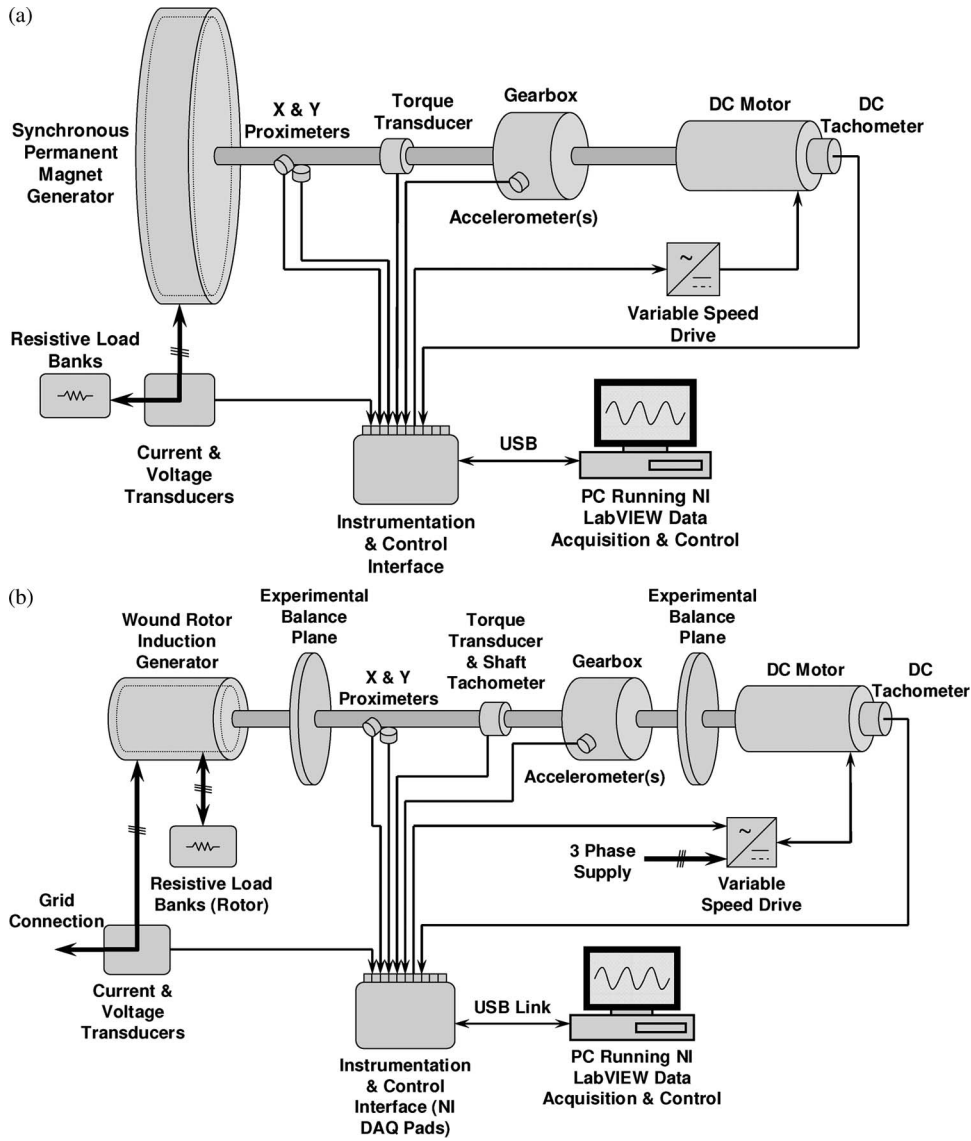


Fig. 6. Schematic diagrams of the WT drive train test rig. (a) With permanent-magnet synchronous generator installed. (b) With induction generator installed.

316 A. WT Drive Train Test Rig

317 One of the difficulties in gaining practical industry experi-
 318 ence of condition monitoring on real WTs is the lack of collab-
 319 oration needed with WT operators and manufacturers, due to
 320 data confidentiality, particularly when faults are present. This
 321 can be avoided by gaining condition monitoring experience
 322 using a controllable experimental test rig to which defined faults
 323 can be applied. Therefore, the technique proposed in this paper
 324 has been validated experimentally on a WT drive train test
 325 rig designed to investigate condition monitoring signals in the
 326 laboratory. This test rig was described in detail in [16] and was
 327 equipped first with a permanent-magnet synchronous generator
 328 and, subsequently, with an induction generator, both as shown
 329 in Fig. 6.

330 The synchronous generator [Fig. 6(a)], such as might be used
 331 in a direct-drive WT, was rated for the experiment at 10 kW,
 332 three-phase 54-pole permanent-magnet machine with a rectified
 333 output feeding a resistive load bank.

The induction generator [Fig. 6(b)], such as might be used
 in a geared-drive WT, was rated for the experiment at 30 kW,
 three-phase four-pole wound-rotor machine, with the rotor cir-
 cuit coupled via slip rings to a three-phase resistive load bank,
 so that rotor electrical imbalance could be applied, and the
 generator stator fed the three-phase mains.

The test rig comprises a 54-kW dc variable-speed motor
 and a two-stage gearbox, instrumented and controlled using
 LabVIEW. In the experiments, a variety of wind speed inputs
 could be applied to the test rig via the dc motor, the speed
 of which is controlled by an external model incorporating the
 properties of natural wind at a variety of speeds and turbulences
 and the mechanical behavior of a 2-MW WT operating under
 closed-loop conditions. Relevant signals were collected from
 the terminals of the generator and the drive train when subjected
 to this driving speed.

A number of electrical and mechanical drive train faults
 could be applied to the test rig. Because they are not necessarily

AQ8

AQ7

precise replicas of WT faults, they have been called “fault-like perturbations” but contain similarities with faults on real WTs. In this paper, to verify the efficacy of the proposed condition monitoring technique for WTs, two “faultlike perturbations” were applied to two different generator configurations as follows.

- 1) In the first configuration, with the synchronous generator representing a direct-drive WT, the “faultlike perturbation” applied was mechanically unbalanced on the generator rotor, representing the effect of a mechanical unbalance fault on the WT generator drive train.
- 2) In the second configuration, with the slip-ring induction generator representing a geared-drive WT, the “fault-like perturbation” applied was electrically asymmetric on the generator rotor, representing the effect of a rotor winding fault, brush imbalance, or air gap eccentricity in the WT generator.

Details of both experimental arrangements are described as follows.

B. Mechanical Unbalance Fault Simulated on Rotor of Synchronous Generator

The mechanical unbalance fault was simulated by attaching a 1-kg mass to the generator rotor with an equivalent rotating mass of 290.7 kg, which is $\sim 0.3\%$. This represents a balance quality grade of $G 7.8$ (7.8 mm/s), within the limit of $G 16$ (16 mm/s) prescribed in ISO1940-1:2003 for a low-speed propeller shaft, applicable to a direct-drive WT shaft. The details of this estimation are given in Appendix A. The peak-to-peak measured displacement of the generator shaft changed a little before and after the placement of the unbalanced mass, varying in the range 90–140 μm . The equivalent vibration velocity would have been 0.13–0.21 mm/s, with the generator running at the maximum rotational speed of 28 r/min well within the 0.71-mm/s limit that is acceptable for machines ≤ 15 kW prescribed in ISO2372:1974.

When the synchronous generator ran at varying speed representing the wind driving situation, the speed, torque, and total power were measured using a sampling frequency of 1 kHz, and the “fault-like perturbation” was periodically applied to the rotor. The time waveforms of the signals before and after the application are shown in Fig. 7(a).

From Fig. 7(a), it can be seen that, in the presence of the mass unbalance fault, the driving shaft torque signal gave a response at the shaft rotational frequency f_{rm} , as expected, fluctuating by 8% range due to the combined effects of mass unbalance fault and wind driving turbulence, which can be compared to fluctuating by 4% due to the wind driving turbulence alone. By contrast, the generator power showed only a slight change in the presence of the fault. In this case, the fault-related frequency is f_{rm} , and the CWT-based energy tracking technique was applied to extract energy at this frequency, as shown in Fig. 7(b). This provided a clear indication of the presence or absence of the mechanical unbalance fault despite the fact that the shaft speed was varying continuously throughout the experiment and the effect could not be observed in the unprocessed total power signal shown in Fig. 7(a).

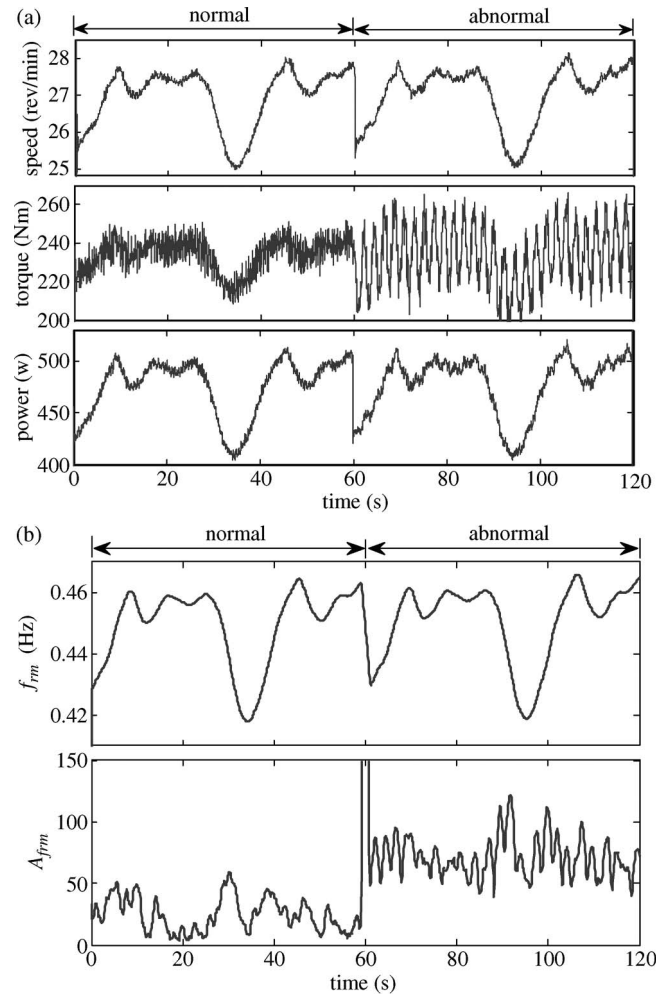


Fig. 7. Mass unbalance fault applied to a synchronous generator rotor on the WT test rig, representing a direct-drive WT. (a) Signals when a mass unbalance fault was simulated on a synchronous generator rotor. (b) Detecting a mass unbalance fault from the power signal.

TABLE II
PARAMETERS USED FOR CALCULATION RESULTS IN FIG. 7

ω_c	ω_f	T
ω_{rm}	$0.03 \omega_{rm}$	$0.2s$

It can be seen from Fig. 7(b) that a 0.3% or $G 7.8$ unbalance fault was easily detectable. This shows that the proposed technique has the potential to detect an incipient mechanical unbalance fault of 0.3% or $G 7.8$ on a direct-drive WT. The parameters used for this calculation are given in Table II.

C. Electrical Asymmetry on Rotor of Induction Generator

The electrical asymmetry was simulated on the induction generator by adjusting the phase resistances in the load bank externally connected to the rotor. Two levels of rotor asymmetry were applied to investigate the effect of an incipient fault. These were an electrical asymmetry of $U_e = 4.7\%$ and, then, a larger asymmetry of 9.2%. The details of the rotor circuit and the estimation of asymmetry are described in Appendix B and in Table IV.

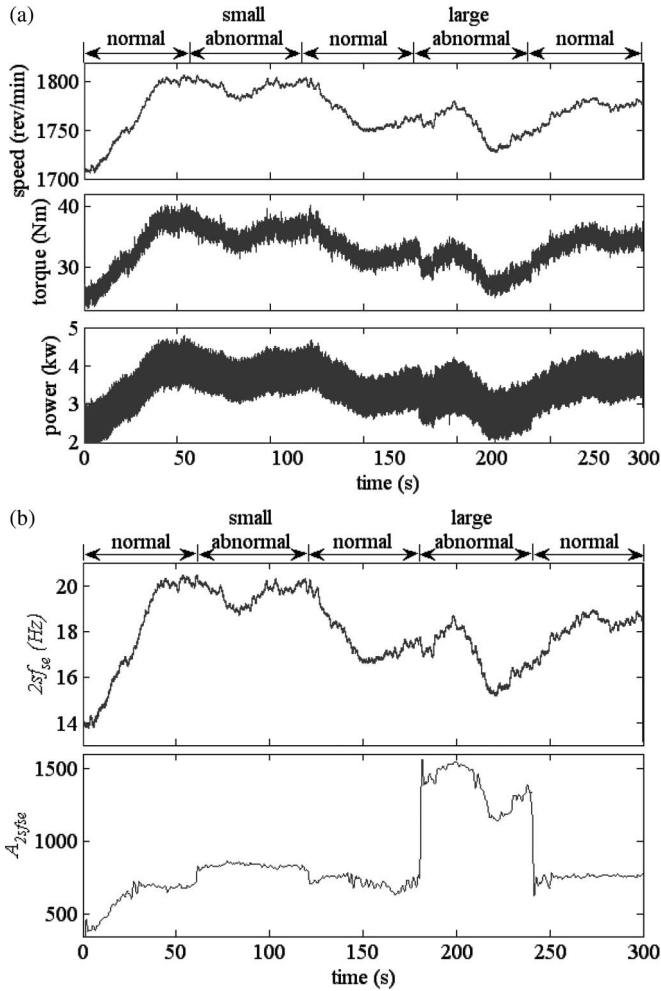


Fig. 8. Electrical asymmetry applied to an induction generator rotor on the test rig, representing a geared-drive WT. (a) Signals when an electrical asymmetry fault was simulated on an induction generator rotor. (b) Detecting an electrical asymmetry fault from the power signal.

As in the mechanical unbalance experiment, the rotational speed, mechanical drive shaft torque, and generator total power signals were measured when the “faultlike perturbation” was periodically applied to the rotor. A smaller fault was applied in the period 60–120 s and a larger fault between 180 and 240 s, with the rotor circuits being balanced in the periods 0–60 s, 120–180 s, and 240–300 s. The time waveforms of the signals collected in this experiment are shown in Fig. 8(a), and it can be seen that, due to the effect of the varying generator speed, the fault symptom cannot be observed clearly from either the generator shaft torque or total power.

When the rotor phase resistances are imbalanced, the generator current, voltage, and power are modulated twice by the slip frequency as the rotor asymmetry moves through the air gap magnetic field twice for every pole pair cycle [4]. Therefore, in this case, the fault-related frequency is $2sf_{se}$, and the CWT-based energy tracking technique was applied to extract the energy at that frequency, as shown in Fig. 8(b).

From Fig. 8(b), it can be seen that the smaller, 4.7%, fault was not clear although it is still visible, so the condition monitoring algorithm had limited detectability in this case. This lack of detectability was due to the residual imbalances present in the

TABLE III
PARAMETERS USED FOR CALCULATION RESULTS IN FIG. 8

ω_c	ω_f	T
$2sf_{se}$	$0.4sf_{se}$	$0.12s$

rotor windings, brush gear, and connections, as well as the negative influence of the timely varying generator rotational speed which partially hid the faulty feature. However, the larger 9.2% fault was clearly visible in the figure and, therefore, readily detectable despite the fact that the $2sf_{se}$ frequency signal was varying during the experimental processes.

This shows that the proposed technique has the potential to detect an incipient 9.2% electrical asymmetry fault on a geared-drive WT generator. The parameters used for this calculation are given in Table III.

V. CONCLUSION

To improve the WT availability and reduce the O&M costs, a new WT condition monitoring technique has been proposed. From this research, the following conclusions can be reached.

- In comparison with the conventional vibration, temperature measurement, and lubrication oil analysis, the technique proposed shows the following potential advantages:
 - reduced capital cost;
 - ability to detect both electrical and mechanical faults;
 - applicable to both geared and direct-drive WTs.
- The proposed CWT-based energy tracking method not only reduces the calculation needed to extract features from lengthy online data but also provides a feasible condition monitoring approach that is applicable to WTs operating at either fixed or variable speed.
- Experiments have shown that the proposed technique is capable of detecting both mechanical and electrical faults in WT drive trains of different types.
- The technique is a feasible way to establish a simple, cheap, but potentially global cost-effective CMS for a WT.

The technique now needs to be applied to the power signals obtained from real WTs during real mechanical and electrical faults to determine the detectability of the algorithm and its ability to detect incipient faults in both cases.

Further work will also be needed to establish the ability of this technique for a wider range of faults and for a variable-speed WT under closed-loop control.

APPENDIX A GENERATOR ROTOR MECHANICAL UNBALANCE

Based on BS ISO1940-1:2003, the balance quality grade G may be calculated by

$$G = e \cdot 2\pi f_{rm} \quad (A1)$$

where

$$e = mr/M_{eq} \quad (A2)$$

$$U_m = (m/M_{eq}) \times 100. \quad (A3)$$

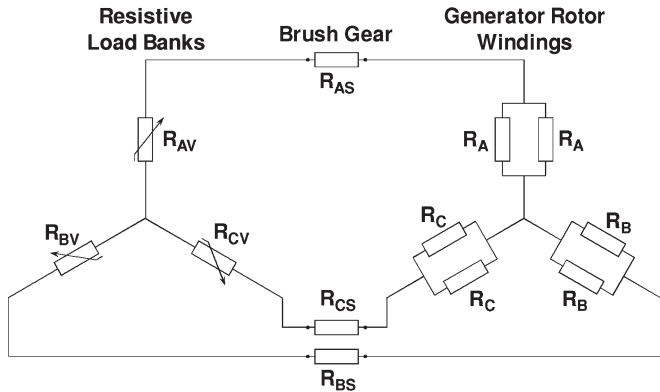


Fig. 9. Rotor circuit diagram, including a resistive load bank.

TABLE IV
ELECTRICAL ASYMMETRY APPLIED TO TEST RIG IN FIG. 8

Time (s)	Description	U_e (%)
0 – 60s	Balanced	0.0
60 – 120s	Low asymmetry	4.7
120 – 180s	Balanced	0.0
180 – 240s	High asymmetry	9.2
240 – 300s	Balanced	0.0

489 For the test rig shown in Fig. 6(a), the unbalance mass $m =$
490 1.0 kg, the effective radius $r = 865$ mm, and the equivalent
491 rotating mass of the test rig $M_{eq} = 290.7$ kg. The average
492 rotational speed of the generator rotor is 25 r/min. This gives
493 a balance quality grade and mechanical unbalance for Fig. 7 of
494 $G 7.8$ ($G = 7.8$ mm/s) and $U_m = 0.3\%$, respectively.

APPENDIX B

GENERATOR ROTOR ELECTRICAL ASYMMETRY

497 The details of the generator rotor circuit shown in Fig. 6(b)
498 taking into account the external resistive load bank are shown
499 in Fig. 9.

500 The balanced circuit resistances were given by

$$\begin{cases} R_{AB} = R_{AV} + R_{BV} + R_{AS} + R_{BS} + (R_A + R_B)/2 \\ R_{BC} = R_{BV} + R_{CV} + R_{BS} + R_{CS} + (R_B + R_C)/2 \\ R_{CA} = R_{CV} + R_{AV} + R_{CS} + R_{AS} + (R_C + R_A)/2. \end{cases} \quad (\text{B1})$$

501 The circuits are balanced, giving

$$R_{AB} = R_{BC} = R_{CA} = \bar{R} = 7.60 \Omega \quad (\text{B2})$$

AQ10 502 where $\bar{R} = (R_{AB} + R_{BC} + R_{CA})/3$.

503 Then, the electrical imbalance can be estimated through
504 calculating the residual circuit resistance δR , i.e.,

$$\delta R = |R_{AB}e^{i\theta_1} + R_{BC}e^{i\theta_2} + R_{CA}e^{i\theta_3}| \quad (\text{B3})$$

505 where $i = \sqrt{-1}$, $\theta_1 = 0$, $\theta_2 = 2\pi/3$, and $\theta_3 = 4\pi/3$.

506 The percentage fault can be described by

$$U_e = (\delta R/\bar{R}) \times 100. \quad (\text{B4})$$

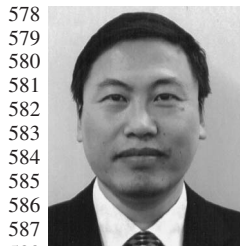
The larger the value of U_e , the more serious the electrical
507 asymmetry. The electrical asymmetries applied in Fig. 8 are
508 listed in Table IV. 509

ACKNOWLEDGMENT

The authors would like to thank the New and Renewable En-
511 ergy Centre, Blyth, for the assistance for the original provision
512 of the test rig. 513

REFERENCES

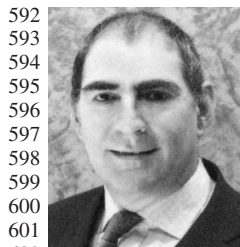
- [1] J. F. Manwell, A. L. Rogers, and J. G. McGowan, "Status of offshore wind
515 energy in the United States," in *Proc. IEEE Power Eng. Soc. Summer*
516 *Meeting*, Jul. 15–19, 2001, vol. 1, pp. 10–13. 517
- [2] H. Polinder, F. F. A. van der Pijl, G. J. de Vilder, and P. J. Tavner, "Com-
518 parison of direct-drive and geared generator concepts for wind turbines,"
519 *IEEE Trans. Energy Convers.*, vol. 21, no. 3, pp. 725–733, Sep. 2006. 520
- [3] J. Nilsson and L. Bertling, "Maintenance management of wind power
521 systems using condition monitoring systems—Life cycle cost analysis for
522 two case studies," *IEEE Trans. Energy Convers.*, vol. 22, no. 1, pp. 223–
523 229, Mar. 2007. 524
- [4] P. J. Tavner, "Review of condition monitoring of rotating electrical ma-
525 chines," *IET Elect. Power Appl.*, vol. 2, no. 4, pp. 215–247, Jul. 2008. 526
- [5] D. Casadei, F. Filippetti, A. Yazidi, C. Rossi, and G. A. Capolino, "Diag-
527 nostic technique based on rotor modulating signals signature analysis for
528 doubly fed induction machines in wind generator systems," in *Conf. Rec.*
529 *IEEE IAS Annu. Meeting*, Oct. 8–12, 2006, vol. 3, pp. 1525–1532. 530
- [6] A. Bellini, F. Filippetti, C. Tassoni, and G. A. Capolino, "Advances in di-
531 agnostic techniques for induction machines," *IEEE Trans. Ind. Electron.*,
532 vol. 55, no. 12, pp. 4109–4126, Dec. 2008. 533
- [7] P. Caselitz and J. Giehardt, "Rotor condition monitoring for improved
534 operational safety of offshore wind energy converters," *Trans. ASME, J.*
535 *Sol. Energy Eng.*, vol. 127, no. 2, pp. 253–261, May 2005. 536
- [8] F. Spinato, P. J. Tavner, G. J. W. van Bussel, and E. Koutoulakos, "Reli-
537 ability of wind turbine subassemblies," *IET Renew. Power Gener.*, vol. 3,
538 no. 4, pp. 1–15, 2009. 539
- [9] S. F. Legowski, A. H. M. Sadrul Ula, and A. M. Trzynadlowski, "Instanta-
540 neous power as a medium for the signature analysis of induction motors,"
541 *IEEE Trans. Ind. Appl.*, vol. 32, no. 4, pp. 904–909, Jul./Aug. 1996. 542
- [10] W. Q. Jeffries, J. A. Chambers, and D. G. Infield, "Experience with
543 bicoherence of electrical power for condition monitoring of wind turbine
544 blades," *Proc. Inst. Elect. Eng.—Vis. Image Signal Process.*, vol. 145,
545 no. 3, pp. 141–148, Jun. 1998. 546
- [11] W. Yang, P. J. Tavner, C. J. Crabtree, and M. Wilkinson, "Research on a
547 simple, cheap but globally effective condition monitoring technique for
548 wind turbines," presented at the XVIII Int. Conf. Electrical Machines
549 (ICEM), Vilamoura, Portugal, Sep., 2008, Paper ID 1053. 550
- [12] J. Cusido, L. Romera, J. A. Ortega, J. A. Rosero, and A. E. Garcia, "Fault
551 detection in induction machines using power spectral density in wavelet
552 decomposition," *IEEE Trans. Ind. Electron.*, vol. 55, no. 2, pp. 633–643,
553 Feb. 2008. 554
- [13] A. Ordaz-Moreno, R. de Jesus Romero-Troncoso, J. A. Vite-Frias,
555 J. R. Rivera-Gillen, and A. Garcia-Perez, "Automatic online diagnosis
556 algorithm for broken-bar detection on induction motors based on discrete
557 wavelet transform for FPGA implementation," *IEEE Trans. Ind. Electron.*,
558 vol. 55, no. 5, pp. 2193–2202, May 2008. 559
- [14] M. Riera-Guasp, J. A. Antonino-Daviu, M. Pineda-Sanchez,
560 R. Puche-Panadero, and J. Perez-Cruz, "A general approach for the
561 transient detection of slip-dependent fault components based on the
562 discrete wavelet transform," *IEEE Trans. Ind. Electron.*, vol. 55, no. 12,
563 pp. 4167–4180, Dec. 2008. 564
- [15] S. S. Tsai, C. T. Hsieh, and S. J. Huang, "Enhancement of damage-
565 detection of wind turbine blades via CWT-based approaches," *IEEE*
566 *Trans. Energy Convers.*, vol. 21, no. 3, pp. 776–781, Sep. 2006. 567
- [16] W. Yang, P. J. Tavner, and M. Wilkinson, "Condition monitoring and
568 fault diagnosis of a wind turbine synchronous generator drive train," *IET*
569 *Renew. Power Gener.*, vol. 3, no. 1, pp. 1–11, Mar. 2009. 570
- [17] E. Wiggelinkhuizen, T. Verbruggen, H. Braam, L. Rademakers, J. Xiang,
571 and S. Watson, "Assessment of condition monitoring techniques for off-
572 shore wind farms," *Trans. ASME, J. Sol. Energy Eng.*, vol. 130, no. 3,
573 pp. 1–9, Aug. 2008. 574
- [18] S. K. Lee, "An acoustic decay measurement based on time–frequency
575 analysis using wavelet transform," *J. Sound Vib.*, vol. 252, no. 1, pp. 141–
576 153, Apr. 2002. 577



Wenxian Yang received the Ph.D. degree in mechanical engineering from Xi'an Jiaotong University, Xi'an, China, in 1999. He completed his postdoctoral research in Northwestern Polytechnical University, Xi'an, in 2001.

He was with the City University of Hong Kong, Kowloon, Hong Kong; Nottingham Trent University, Nottingham, U.K.; Cranfield University, Cranfield, U.K.; and Durham University, Durham, U.K. He is currently a Technical Specialist with the New and Renewable Energy Centre, Blyth, U.K. He has

worked in the areas of new and renewable energy, signal processing, machine condition monitoring and fault diagnosis, nondestructive testing and nondestructive evaluation, and artificial intelligence in both industry and academia.



Peter J. Tavner (SM'08) received the M.A. degree from Cambridge, U.K., in 1969 and the Ph.D. degree from Southampton, U.K., in 1978.

He held research and technical positions in the industry, including Group Technical Director with FKI Energy Technology, Loughborough, U.K. He is currently the Head of the School of Engineering and Computing Sciences, Durham University, Durham, U.K., and a Professor with the New and Renewable Energy Centre, Blyth, U.K. His research interest includes machines for renewable energy, condition

monitoring, and reliability. Dr. Tavner was the recipient of the Institution Premium of the Institution of Electrical Engineers, U.K.



Christopher J. Crabtree received the M.S. degree in engineering from Durham University, Durham, U.K., in 2007 having studied new and renewable energy as an electrical engineer, where he is currently working toward the Ph.D. degree in condition monitoring of offshore wind turbines.

His research interests include the development of condition monitoring techniques using industrial data and a test rig.

AQ16

606

607

608

609

610

611

612

613

614



Michael Wilkinson received the M.Sc. degree in electromagnetic sensing from Durham University, Durham, U.K., in 2003 and the Eng.D. degree with a thesis on condition monitoring for offshore wind turbines from Newcastle University, Newcastle upon Tyne, U.K., in 2007, in a collaborative project with Durham University and FKI Energy Technology.

In 2007, he joined Garrad Hassan, Bristol, U.K., as part of the operational projects team, where he has been monitoring wind farms worldwide on behalf of owners. His research interests include condition monitoring and reliability of wind turbines.

AQ17

615

616

617

618

619

620

621

622

623

624

625

626

AUTHOR QUERIES

AUTHOR PLEASE ANSWER ALL QUERIES

- AQ1 = “EPSRC” was defined as “Engineering and Physical Sciences Research Council.” Please check if appropriate.
- AQ2 = Current affiliation was provided in the first footnote for author Wenxian Yang to be consistent with the current affiliation in the vitae. Please check if appropriate.
- AQ3 = Current affiliation was provided in the first footnote for author Peter J. Tavner to be consistent with the current affiliation in the vitae. Please check if appropriate.
- AQ4 = Current affiliation was provided in the first footnote for author Christopher J. Crabtree to be consistent with the current affiliation in the vitae. Please check if appropriate.
- AQ5 = Current affiliation was provided in the first footnote for author Michael Wilkinson to be consistent with the current affiliation in the vitae. Please check if appropriate.
- AQ6 = Please check if call-out a) in upper left corner of Fig. 1 should be deleted.
- AQ7 = Please check on the edits for this sentence if it is appropriate. Originally, the sentence was “The synchronous generator, Fig. 6(a), was such as might be used in a direct drive WT, rated for the experiment at 10 kW, 3-phase, 54-pole, permanent-magnet machine with a rectified output feeding a resistive load bank.”
- AQ8 = Please check on the edits for this sentence if appropriate.
- AQ9 = “rev/min” was changed to “r/min” for revolution per minute to follow IEEE style. Please check if appropriate.
- AQ10 = “Ohm” was changed to symbol “ Ω .” Please check if appropriate.
- AQ11 = “NDT” was defined as “nondestructive testing.” Please check if appropriate.
- AQ12 = “NDE” was defined as “nondestructive evaluation.” Please check if appropriate.
- AQ13 = Please provide academic institution for the M.A. degree received.
- AQ14 = Please provide academic institution for the Ph.D. degree received.
- AQ15 = “Centre” was added after “New and Renewable Energy,” and address was provided for the center. Please check if appropriate.
- AQ16 = “Masters in Engineering” was changed to “M.S. degree in engineering.” Please check if appropriate.
- AQ17 = Please check if the provided address for Garrad Hassan is correct.

END OF ALL QUERIES